Astronomy & Astrophysics manuscript no. output
June 30, 2022

Asteroid spin-states of a 4 Gyr-old collisional family. ⋆

D. Athanasopoulos[1], J. Hanuš[2], C. Avdellidou[3], R. Bonamico[4], M. Delbo[3], M. Conjat[3], A. Ferrero[5], K. Gazeas[1], J.P. Rivet[3], N. Sioulas[6], G. van Belle[7], P. Antonini[8], M. Audejean[9], R. Behrend[10], L. Bernasconi[11], J.W. Brinsfield[12], S. Brouillard[13], L. Brunetto[14], M. Fauvaud[15], S. Fauvaud[15], R. González[16], D. Higgins[17], T.W.-S. Holoien[18,19], G. Kobber[20], R.A. Koff[21], A. Kryszczynska[22], F. Livet[23], A. Marciniak[22], J. Oey[24], O. Pejcha[25], J.J. Rives[13], and R. Roy[26]

(Affiliations can be found after the references)

June 2022

ABSTRACT

Context. Families of asteroids generated by the collisional fragmentation of a common parent body have been identified using clustering methods of asteroids in their proper orbital element space. However, there is growing evidence that some of the real families are larger than the corresponding cluster of objects in orbital elements, as well as there are families that escaped identification from clustering methods. An alternative method has been developed in order to identify collisional families from the correlation between the asteroid fragment sizes and their proper semimajor axis distance from the family center (V-shape). This method has been shown to be effective in the cases of the very diffuse families that formed Gyrs ago.

Aims. Here we use multiple technique observations of asteroids to provide corroborating evidence that one of those groups of asteroids identified as a family from the correlation between size and proper semimajor axis of asteroids are real fragments of a common parent body and, thus form a collisional family.

Methods. We obtained photometric observations of asteroids in order to construct their rotational lightcurves, we combine these with literature lightcurves and sparse-in-time photometry, we input these data in the so-called lightcurve inversion methods, which allow us to determine a convex approximation to the 3D shape of the asteroids and their orientation in space; from the latter we extract the latitude (or obliquity) of the spin pole in order to assess whether an object is prograde or retrograde. We included in the analysis spin pole solutions already published in the literature aiming to increase the statistical significance of our results. The ultimate goal is to assess whether we find an excess on retrograde asteroids in the inward side of the V-shape of a 4-Gyr old asteroid family identified by Delbo' et al. (2017) with the V-shape method. This excess of retrograde rotators is predicted by the theory of asteroid family evolution.

Results. We obtained the latitude of the spin poles for 55 asteroids claimed to belong to a 4 Gyr-old collisional family of the inner main belt that consists of low-albedo asteroids. After having re-evaluated the albedo and spectroscopic information, we found that nine of the aforementioned asteroids are interlopers in the 4 Gyr-old family. Of the 46 remaining asteroids, 31 are found to be retrograde, whereas 15 prograde. We also found that this excess of retrograde rotators have very low probability (1.29%) to be due to random sampling from an underling uniform distribution of spin poles.

Conclusions. Our results constitute a corroborating evidence that the asteroids identified by Delbo' et al. (2017) as members of a 4 Gyr-old collisional family, have a common origin, thus strengthening their family membership.

Key words. minor planets, asteroids: general – astronomical databases: miscellaneous

1. Introduction

The study of asteroid families has been an active research field since the discovery of the first groupings of asteroids in orbital element space (Hirayama 1918). As more asteroids were discovered, these initial groupings became more numerous, thus substantiating their significance. At the same time, more asteroid groupings, i.e. families, were discovered. Studies of the physical properties of asteroids also highlighted that the families were also homogenous in colours, albedo, and spectral properties, in general (see Masiero et al. 2015, for a review). This fact corroborated the idea that these groups of asteroids in orbital element space were fragments of a common parent body. This is the reason why they are also called collisional asteroid families (see Nesvorný et al. 2015, for a review on the subject).

The identification of the collisional families has been done using classical methods, such as the hierarchical clustering method (HCM; Zappala et al. 1990, 1995). Surveys of identification of asteroid collisional families have found that about one-third of the known asteroid population is associated with over 120 collisional families (see e.g. the Minor Planet Physical Properties Catalogue (MP3C) [1]. However, it is well known that the large majority of asteroid family identification surveys are conservative in order to well identify the core of the family and keep a good separation between the nearby families as well (Nesvorný et al. 2015).

A very important question is that how many of the asteroids that are included in the so-called "background" population, i.e., that do not belong to families, of the main belt are instead collisional members that have not been associated to known families. There is evidence that this number is very large, implying that (i) collisional families are larger than what is reported in our current catalogues (Brož & Morbidelli 2013; Tsirvoulis et al. 2018; Dermott et al. 2021) and (ii) there are still undiscovered families. This problem derives from the difficulty of linking to the family

⋆ This article is dedicated to the memory of Gianfranco Marcon, whose telescopes have contributed to development of astronomy and to the observations collected for this study.

[1] mp3c.oca.eu

core the collisional members that currently reside far away in orbital elements (Milani et al. 2014). It also been shown that there is unexpected lack of asteroid families that formed more than 2 Gyr years ago from a parent body larger than about 100 km (Brož & Morbidelli 2013). Moreover, Tsirvoulis et al. (2018) attempted to identify families using an aggressive version of the HCM, such that it was very generous in linking large number of asteroids to their respective families. These authors found evidence of undetected family members in the investigated region of the main belt from the study of the size frequency distribution of the non-family members. These observations also corroborate both the aforementioned hypothesis (i) and (ii).

As a collisional family ages, a non-gravitational force, known as the Yarkovsky effect (e.g., the review of Vokrouhlický et al. 2015), pushes asteroids away from the centre of the family with a drift rate da/dt that is proportional to the inverse diameter (1/D), where a is the asteroid orbital semimajor axis. Prograde rotating asteroids have da/dt>0 and move to larger semimajor axis while retrograde ones, with da/dt<0, move to smaller, semi major axis. This creates correlations of points in the (1/D vs. a) plane called V-shapes, as they resemble the letter "V", whose slope (K) indicates the family age. As an asteroid family spreads in orbital semimajor axis, family members cross orbital resonances with planets, which perturb their eccentricity and inclination. Hence, old families are less compact than younger ones in all three proper orbital elements space. This makes old families (whose members have large orbital element spreading) more difficult to be identified by the HCM (e.g., Bolin et al. 2017), and cause families to overlap to each other.

Based on the V-shape characteristic, there has been developed a method (Bolin et al. 2017; Delbo' et al. 2017) to discover old and dispersed asteroid families.This V-shape identification method has been already used to discover five families of the inner main belt: the Eulalia and New Polana families (Walsh et al. 2013), a "primordial" family with a nominal age of $4.0^{+1.7}_{-1.1}$ Gyr, but that could be as old as the Solar System, the Athor family with age $3.0^{+0.5}_{-0.4}$ Gyr and the Zita family with age $5.0^{+1.6}_{-1.3}$ Gyr (Delbo' et al. 2017; Delbo et al. 2019).

Although the V-shape family identification method is indeed a powerful tool, its efficiency also decreases with increasing family age (Deienno et al. 2021) due to the fact that the most dispersed family members cannot be distinguished anymore from the background, the latter possibly also consisting of old and dispersed overlapping families. Given the current limitations of the detection methods, we seek for independent ways to confirm family members and thus the borders of the families identified on the basis of their V-shapes. One of these independent methods is to check the spin state of the family members. According to the aforementioned theory of the Yarkovsky effect, it is expected that most of the asteroids in the inward side (the left side of the V) of the family are retrograde, and prograde in the outward side (the right side of the V). This has been shown to work in notable HCM asteroid families (Hanuš et al. 2013a, 2018).

One of the most effective techniques to identify the spin state of asteroids is the inversion of their photometric lightcurves (Kaasalainen & Torppa 2001; Kaasalainen et al. 2001). This method requires the acquisition of large datasets of photometric measurements, where most of them are currently retrieved from all-sky surveys. However, such data are sparse in time by nature and often do not allow unambiguous determination of asteroid rotational period due to their low photometric accuracy of typically 0.1 magnitude. Often, addition of classical, dense-in-time, optical lightcurves to the sparse dataset leads to the removal of such ambiguity.

In this work we study the spin states of asteroids that belong to the innermost border of the inward side of a primordial family of the inner main belt that was reported by Delbo' et al. (2017). This primordial family has orbital elements (a, e, i) roughly $(2.26, 0.14, 5.75°)$ for the inward wing as only this has been identified and is suspected to contain low-albedo carbonaceous/C-complex asteroids. For this, we run our own observing program (called *Ancient Asteroids*) and obtain dense-in-time lightcurves, which we combine with existing sparse-in-time photometric data.

In Sec. 2, we present optical datasets used in this work and present our observing campaign. In Secs. 3 and 4, we describe the lightcurve inversion method used for the analysis of the optical data and for the determination of asteroidal physical properties. In Sec. 5 we present our results on the spin poles of our dataset indicating also the potential asteroid interlopers of the primordial family, while in Sec. 6 we discuss the results.

2. Datasets

In order to verify membership in the primordial family, we focus our analysis on the asteroids that are located between the inward border of the primordial family and the respective border of the Polana family (see Fig. 1). The latter, which is also called New Polana after its reassessment by Walsh et al. (2013), is another large but younger, family in the inner main belt of similar carbonaceous composition and low albedo. We use the families' V-shapes of Walsh et al. (2013) and Delbo' et al. (2017) to delimit the two families. This group of objects should belong either to the vast and extensive primordial family or to the unidentified background population. In order to study the spin poles of the primordial family we combined a plethora of data. These include (i) asteroid lightcurves that we collected from the databases, (ii) sparse photometric data obtained from different surveys, (iii) existing complete or incomplete shape models, and (iv) our own photometric observations.

2.1. Currently available asteroid models

The vast majority of asteroid shape models has been produced by the lightcurve inversion method (Kaasalainen & Torppa 2001; Kaasalainen et al. 2001). The Database of Asteroid Models from Inversion Techniques (DAMIT)[2] contains ∼6 000 asteroid models for ∼3 460 asteroids (March 2022) that are publicly available (Durech et al. 2010). Shape models for 15 asteroids from our list are already included in DAMIT (see Table B.1). Furthermore, we also considered the so-called partial models published in Ďurech et al. (2020). For the latter models, only the sidereal rotation period, ecliptic latitude of the spin axis and its range are reported. This information is sufficient for our purposes, as it often allows us to securely decide whether the asteroid is a prograde or a retrograde rotator.

2.2. Archival photometric data

Photometric data of asteroids are scattered throughout various public databases or were provided to us directly by the observers. During the past two decades, a large internal database of optical lightcurves is maintained at the Institute of Astronomy of Charles University that is routinely used for shape modeling. A large amount of data was obtained from the Aster-

[2] https://astro.troja.mff.cuni.cz/projects/damit/

oid Lightcurve Data Exchange Format (ALCDEF) database[3] (Stephens & Warner 2018) (147 dense photometric lightcurves that exist for 19 of our asteroid targets). Additional dense lightcurves were downloaded from the Asteroid Photometric Catalogue (APC; Lagerkvist & Magnusson 2011), the Courbes de rotation d'astéroïdes et de comètes database (CdR[4]) or provided directly by the observers (see Table B.2).

The sparse-in-time data that come from various sky-surveys were obtained from corresponding databases and archives connected to the publications. We used data from the US Naval Observatory in Flagstaff (USNO-Flagstaff, IAU code 689), the Catalina Sky Survey (CSS, IAU code 703; Larson et al. 2003), Gaia Data Release 2 (GaiaDR2; Gaia Collaboration et al. 2018), the All-Sky Automated Survey for Supernovae (ASAS-SN; Shappee et al. 2014; Kochanek et al. 2017; Hanuš et al. 2021), the Asteroid Terrestrial-impact Last Alert System (ATLAS; Tonry et al. 2018; Ďurech et al. 2020), the Zwicky Transient Facility (ZTF, IAU code I41; Bellm et al. 2019), the Palomar Transient Factory Survey (PTF; Chang et al. 2015; Waszczak et al. 2015), and TESS (Ricker et al. 2015; Pál et al. 2020). Tables B.3 and B.4 summarise the typical amount of measurements from these surveys that were available for our targets. In general, data from USNO-Flagstaff, GaiaDR2, ZTF, TESS and PTF are rather limited for our targets, while hundreds of individual measurements are available from CSS, ASAS-SN and ATLAS surveys. CSS, USNO-Flagstaff and ZTF data were obtained through the AstDys-2 database[5].

2.3. ASAS-SN *g*-band data

As discussed in Sec. 2.2, we use *V*-band sparse data from the ASAS-SN survey through the catalogue of Hanuš et al. (2021). However, since 2018 ASAS-SN has switched to the SLOAN *g* filter and significantly expanded to more telescope units and sites, we utilised these data in our work as well. We accessed and processed the *g*-band data following the same procedure as in Hanuš et al. (2021). The time coverage is already more than three years. Moreover, the *g*-band limiting magnitude is larger by about one magnitude than in the *V*-band. Therefore, the *g*-band dataset is often comparable in the means of the number of measurements to the *V*-band dataset for brighter objects, and outperforms the *V*-band dataset for fainter objects. Both filters are treated independently in the shape modelling.

2.4. Ancient Asteroids: An international observing campaign

In order to enlarge our input dataset used for the shape modelling, which would potentially lead to new and improved shape solutions, we performed additional ground-based photometric observations. An international observing campaign has been initiated in the framework of our international initiative called *Ancient Asteroids*[6], in order to collect dense photometric data for asteroids that belong to the oldest asteroid families (Athanasopoulos et al. 2021). *Ancient Asteroids* establishes a network of astronomers, currently from four countries, who follow a common observing plan. In the following we present the observing facilities and their corresponding equipment that participated in this work and provided data for 33 asteroids of our dataset.

[3] https://alcdef.org/
[4] https://obswww.unige.ch/~behrend/page3cou.html
[5] https://newton.spacedys.com/astdys/
[6] http://users.uoa.gr/~kgaze/ancient_asteroids.html

Astronomical Observatory BSA

BSA is an amateur observatory located in Savigliano, Italy. BSA used for this study a robotic 0.3 m (f/8) Ritchey-Chretien telescope and an open-filter SBIG ST-9 XME CCD detector.

Lowell Observatory

Lowell is located in Arizona, United States and for this project it operated two robotic telescopes. These were the Titan Monitor Telescope (TiMo), a 20" PlaneWave CDK20 telescope equipped with a Moravian instruments G3-6300 CCD detector, as welll as a 1 m PlaneWave (PW1) telescope equipped with a Finger Lakes Instruments ML-16803 CCD imager. TiMo is located on Lowell's main Mars Hill campus (IAU Code 690), whereas the PW1 is on Lowell's Anderson Mesa campus (IAU Code 688). All the observations were performed in Sloan r' filter.

Bigmuskie Observatory

It is an amateur observatory located in Mombercelli-Asti, Italy. Bigmuskie utilises a 40 cm (f/8.25) Ritchey- Chrétien telescope. The observations were performed unfiltered by using a Moravian G3-1000 CCD detector.

Observatoire de la Côte d'Azur (OCA)

The observations were performed at the C2PU facility in Calern, which belongs to the Observatoire de la Côte d'Azur in France, at an altitude of a 1300 m. C2PU operated the 1.04 m Cassegrain telescope ("Omicron@C2PU") with an f/3.2 parabolic, prime focus and with a 3-lenses Wynne coma corrector using an unfiltered QHY600 CMOS camera (Bendjoya et al. 2012).

University of Athens Observatory (UOAO)

The UOAO belongs to the National and Kapodistrian University of Athens in Greece, which utilises a robotic 0.4 m (f/8) Cassegrain telescope equipped with an SBIG ST-10 XME CCD detector (Gazeas 2016). All the observations were performed unfiltered.

Helmos Observatory

Helmos observatory is operated by the National Observatory of Athens and is located on mount Helmos (Aroania) in Greece, at an altitude of 2340 m. It utilises a robotic 2.3 m (f/8) Ritchey-Chrétien telescope ("Aristarchos") (Goudis et al. 2010). All the observations were performed unfiltered by using the Princeton Instruments VersArray 2048B LN CCD camera.

NOAK Observatory

NOAK observatory is located in the city of Ioannina, Greece. It utilises a 0.25 m (f/4.7) robotic Newtonian telescope. All the observations were performed unfiltered by using an ATIK 460EXM CCD camera.

BlueEye 600 Observatory (BE600)

BlueEye 600 robotic observatory (BE600) is operated by the Astronomical Institute of the Charles University and located in Ondřejov, Czech Republic. It utilises a 60 cm Ritchey-Chrétien

telescope (Officina Stellare). All the observations were performed by Martin Lehký[7] utilizing the standard Johnson R filter and the E2V42–40 CCD camera (Ďurech et al. 2018b).

Pic de Château-Renard Observatory (ChR)

Pic de Château-Renard Observatory (2936 m altitude, Saint-Véran, French Alps) is a facility operated by the Paris-Meudon Observatory and AstroQueyras, an amateur association. Observations were performed unfiltered by using a 0.5 m (f/8) Ritchey-Chrétien telescope equipped with a SBIG STX 16803 camera.

Observatoire du Bois de Bardon (OBdB)

OBdB is an amateur observatory located in Taponnat, France. OBdB used a 0.28 m (f/3) Schmidt-Cassegrain telescope equipped with a SBIG ST-402 ME CCD camera. Observations were performed with an r' (Sloan) filter.

Blue Mountains Observatory

Blue Mountains Observatory is located at an altitude of 900m in Leura, Australia. The photometric observations are done with Classical Celestron Schmidt Cassegrain Telescope, 0.35 m in diameter operating at f/5. All images are taken unfiltered using SBIG CCD camera ST8-XME at bin 1x1.

3. Photometric reduction

The photometric datasets used in this work include both dense photometric data from ground-based facilities (retrieved from literature or from our observing campaign), as well as sparse data from several sky surveys and space missions as described before. These two different datasets require different analysis techniques.

3.1. Observations of the program Ancient Asteroids

Our observations were performed mainly in clear filter, in order to increase the signal-to-noise in our lightcurves, while keeping the exposure time as short as possible and increase the sampling frequency. The exposure time was varying between 30 s and 240 s, depending on the brightness of the target, telescope aperture and observing conditions.

The collected data from all observatories were reduced, following the standard image processing procedure of calibration and aperture photometry (e.g., Massey 1997; Gallaway 2020). The calibration was performed for all light frames in three steps, namely, the bias and dark subtraction and the flat-field correction. Aperture photometry is a quite simple technique and most applicable to stellar fields which are relatively sparse. This procedure was compiled by utilising *AIP4Win* software (Berry & Burnell 2005) for the fields observed by C2PU, UOAO, Helmos, and NOAK observatories, IRIS software [8] for the images performed by OBdB and ChR observatories, and *MPO Canopus* software (Warner 2015) for the rest (see Table B.5).

The differential photometry was performed either with five bright field stars or by estimating an artificial comparison star, following the methodology presented by Broeg et al. (2005). The resulting measurements were provided in differential magnitudes with a photometric accuracy of 0.02–0.1 mag. In the case of OBdB and ChR observatories, the differential photometric data were performed by estimating an artificial comparison star following the methodology described by (Fauvaud & Fauvaud 2013, 2014).

We performed the σ-clipping method (see, Gallaway 2020) for removing the prominent outliers in our measurements, which were usually caused by cosmic rays or satellite passing through the field. In case where the asteroid was passing near a field star within a range of an aperture size (typically of the order of 5-7 arcseconds) we trimmed the lightcurve and we kept only the "clear" parts.

We used the Pogson equation ($m = -2.5log(F) + c$) to transform the differential magnitude (m) to relative flux (F). The relative flux values were normalised by defining the average flux of each lightcurve as one. For all the epochs of the observed lightcurves, we performed the light travel time correction (from the asteroid to the observer) and computed the ecliptic Cartesian coordinates (x, y, z) of the Sun and of the Earth, with the asteroid as the reference point, in [au] via the Miriade service (Berthier et al. 2009). Such format is required by the Convex Inversion (CI) method that we used for the shape modeling, as described in Sec. 4.

3.2. Adopted data

The dense photometric data from databases such as Asteroid Lightcurve Data Exchange Format database (ALCDEF) or APC are in magnitude values, so we converted them to relative fluxes by following the same procedure as described in Sec. 3.1.

Apart from dense photometric data, we included also sparse in time photometric measurements from various sources as they proved to be useful in constraining the asteroid models, despite their usually low photometric accuracy of ∼0.1 mag (Ďurech et al. 2009; Hanuš et al. 2011, 2013b; Ďurech et al. 2016). In order to use the sparse data for the shape modelling by the CI method, we processed them following the procedure of Hanuš et al. (2011). For more details, we refer to the most recent description of the procedure applied to ASAS-SN data by Hanuš et al. (2021). All individual measurements within each sparse dataset (i.e., specific survey and photometric filter) are internally calibrated, therefore we process each dataset separately. First, the sparse data are usually available in magnitude values, which we transform into fluxes utilising the Pogson equation and, for convenience, setting the zero magnitude to 15. We then apply the light travel time correction to each epoch. Next, we normalize the fluxes to a referenced one astronomical unit distance of the asteroid to the Earth and the Sun. The final steps were σ-clipping to reject the outliers and estimating relative weights of each sparse data set with respect to the dense data (see Hanuš et al. 2021).

4. Determination of the spin poles

We used the CI method developed by Kaasalainen & Torppa (2001); Kaasalainen et al. (2001). This gradient-based inversion technique is based on shape model parametrisation by a set of facets and their normal vectors and their optimization such that they fit to the observed lightcurves. Assuming a convex shape representation of the asteroid shape, the inversion problem is unique. However, adding the rotation state (i.e., sidereal rotation period and spin axis orientation) as additional free parameters,

[7] Deceased November 18th, 2020.
[8] http://www.astrosurf.com/buil/iris-software.html

we lose the uniqueness of the solution and the parameter space becomes full of local minima. We have to search the parameter space on a grid of input parameters and find the local minimum that corresponds to the global minimum, thus the correct set of searched parameters. The production of the model lightcurve, that is compared by the method to the observed lightcurves, is performed by using an empirical light-scattering model that is a combination of single Lommel-Seeliger and multiple Lambert scattering models (Kaasalainen et al. 2002). So far, the CI has been used to derive asteroid models for more than 3 460 asteroids that are stored in the DAMIT database.

We assume that the shape effects in the light curves are independent on the used photometric filters while covering the reflected-dominated spectral range. Therefore, we can treat all dense light curves as relative, i.e., normalized to unity. Although each sparse data set is, in principle, internally calibrated in a different photometric system, we use the sparse data also as normalized to unity. The only caveat is that we assume that the phase function is the same in each photometric system. This is not fully correct, e.g., Ďurech et al. (2020) found a statistically significant differences in the ATLAS data taken in c and o filters, in accordance with the "phase reddening" effect (Millis et al. 1976; Lumme & Bowell 1981). However, for our purposes it is sufficient to have a single phase function for all sparse datasets.

We combined all available datasets and applied the CI to them. We weighted individual lightcurves and sparse datasets based on their accuracy (expected rms). Individual weights w_i were normalized such that $\sum(w_i) = N$, where N is the number of dense lightcurves plus the number of sparse datasets. The process that we followed is described by Hanuš et al. (submitted to A&A).

4.1. Rotation period

For asteroids with previously known rotation period, we searched for the best-fit model with the period parameter varying between boundaries defined by 5%, 10% and 20% of the previously reported period in the LightCurve DataBase (LCDB; Warner et al. 2009), depending on the reliability flag provided for each period estimate 3 and 3–, 2+, 2. Rotation periods for asteroids with other reliability flags were considered as unknown.

Fourier-based algorithms are unable to efficiently estimate the rotation period of asteroids in cases of only sparse photometric data availability or extreme slow rotators, where their rotation period far exceeds the night duration. In such cases, we performed a dense scanning in the rotation period parameter space from 2 h, which has been observed as a approximate lower limit of (>150 m sized) asteroids by Pravec et al. (2002), up to 5 000 h, which was motivated by the recent discovery of superslow rotating asteroids by Erasmus et al. (2021).

Note that the period search is actually a full shape and rotation state optimization by the CI. However, this procedure was performed on a grid of pole orientations limited to only ten values evenly distributed on a sphere and rather rough shape model resolution. We only recorded the rotation period and the best-fitting rms (and χ^2) value within the grid of pole directions. We considered the best-fitting period searched on selected period interval as unique, if its $\chi^2_{\rm min}$ is the only solution below the threshold defined as

$$\chi^2_{\rm tr} = \left(1 + 0.5\sqrt{\frac{2}{\nu}}\right)\chi^2_{\rm min}, \quad (1)$$

where ν corresponds to the number of degrees of freedom (number of observations minus the number of free parameters).

Interestingly, the difference between two local minima in the period parameter space ΔP is dependent only on the time span of the data T and the sidereal rotation period P itself

$$\frac{\Delta P}{P} = \frac{1}{2}\frac{P}{T}, \quad (2)$$

thus, for instance, independent on the shape resolution. We sample the period with a step of $0.5\Delta P$ that we recompute every step. Note that $\sim 1/20$ of ΔP is a reliable uncertainty for the derived rotation period as it corresponds to a rotation phase offset of about 10°, which is a typical uncertainty of the pole direction.

4.2. Spin pole and shape

After the determination of the rotation period, we applied the CI method on a much denser grid of initial spin directions (ecliptic longitude λ and latitude β) and a higher shape resolution[9]. The best-fitting shape and spin pole solution is considered unique if fulfills the condition of Eq. 1. Most of the cases presented two symmetrical solutions with respect to ecliptic longitude ($\lambda\pm$ 180°), the so-called pole ambiguity (Kaasalainen & Lamberg 2006).

If photometric data are rich enough in observing geometries and have reasonable accuracy relative to the amplitude of the asteroid lightcurve, the unique solution can be often derived. Sometimes, however, the photometric data are insufficient for deriving a unique solution, but they allow us to derive a unique period and 3–4 pole solutions that have similar values of the ecliptic latitude β. These so-called partial models are still useful, especially for our study, as it is possible to decide whether the asteroid is a prograde or a retrograde rotator. Therefore, we made an effort to identify such cases here together with the unique solutions.

5. Results

5.1. New period estimates

We derived improved values of the sidereal rotation period for 29 asteroids, as presented in Tables B.3 and B.4 (see also Fig. A.1 for an example of typical periodograms). All these period values are consistent with the synodic periods reported in the LCDB database[10]. The revised asteroid models have almost the same period as the previous solutions. Moreover, we measured rotation periods for 7 asteroids for the first time. These periods were derived using sparse photometric data. Of these asteroids two are a super-slow rotator with P = 3253.5 h, and a slow rotator with P = 152.62 h, which are (2776) Baikal and (8315) Bajin, respectively. All the others, namely, (12722) Petrarca, (13066) 1991 PM13, (23495) 1991 UQ1, (49863) 1999 XK 104 and (70184) 1999 RU3, are rather fast rotators, with periods between 3 and 10 h.

[9] For the search of the rotation period, we fit 7^2 coefficients of the spherical harmonic expansion and start with 10 different pole directions uniformly distribute on the sphere. On the other hand, the denser grid utilizes 9^2 coefficients of the expansion and 48 input pole directions. The typical polyhedron representing the final shape solution contains about 1,000 vertices and 2,000 facets.

[10] The only exception is asteroid (1159) Granada with the reported LCDB period of 77.28 h. However, this period adopted from the CdR database is preliminary and, for example, inconsistent with the period reported by Waszczak et al. (2015), which is on the other hand similar to the one we derived.

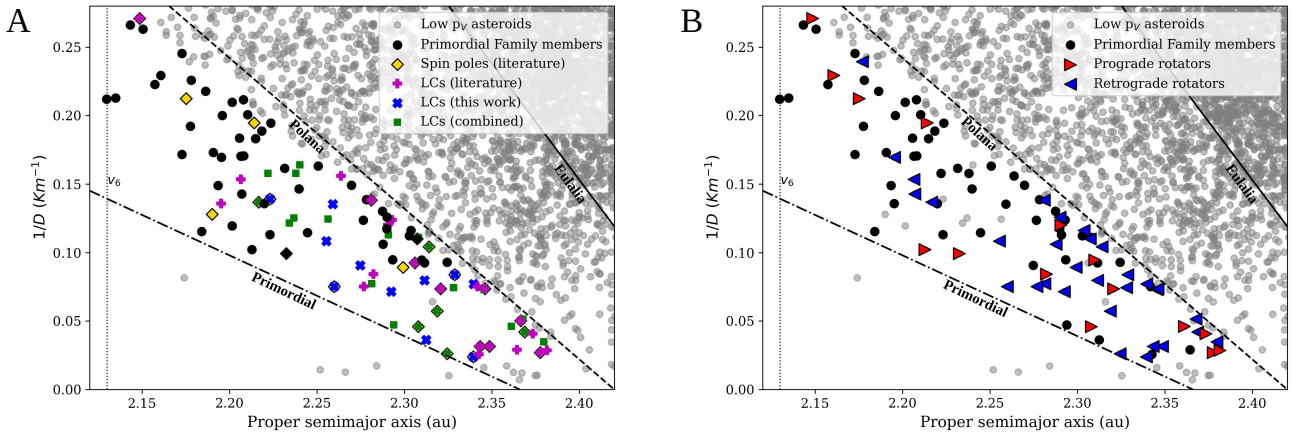

Fig. 1. Panel A: The primordial family members are presented in proper semi-major axis vs. inverse diameter plane, along with the low albedo asteroids located in the innermost region of the Main Belt. Yellow diamond markers present members with known spin pole from the literature. Additionally, "plus", cross and square markers show members from which there are dense lightcurves only from literature, from this work and from both sources, respectively. See more details in Table B.2. Panel B: The left side of the V-shape of the primordial family, where the red markers show the prograde and blue markers the retrograde asteroids, respectively.

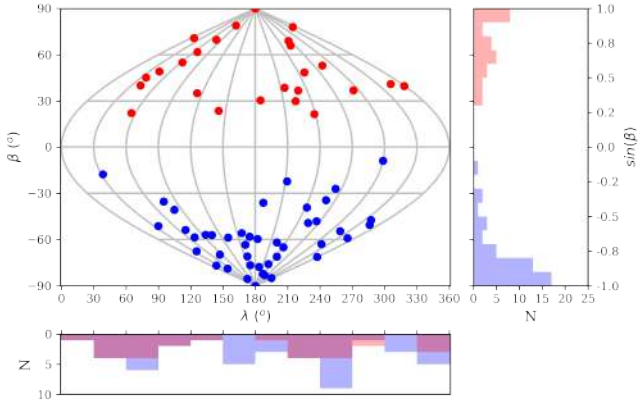

Fig. 2. Distribution of the complete spin pole solutions for the primordial family members. The main plot is a sinusoidal equal-area cartographic representation, where the vertical grey lines define the longitude (λ) and the horizontal curves define the latitude (β). The right histogram represents the latitude (β) of prograde (red) and of retrograde (blue) rotators. The bottom histogram represents the longitude (λ) of prograde (red) and of retrograde (blue) rotators. The specific values for each asteroid are shown in Tables B.3 & B.4.

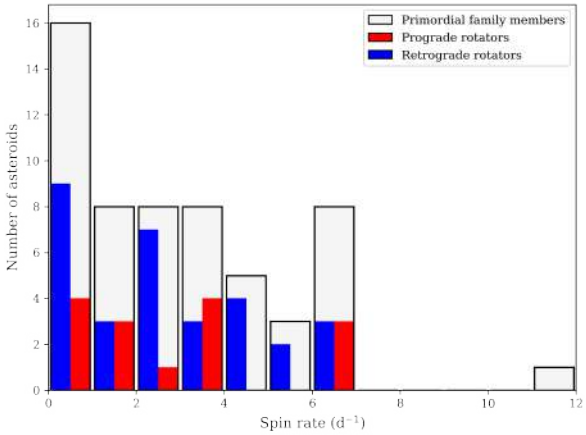

Fig. 3. Histogram of spin rate for members of the primordial asteroid family, where the prograde rotators are denoted with red color and retrograde with blue. The light grey bars represent all primordial family members, whose rotational period is known either from this study or literature.

5.2. Spin pole directions

By combining new and literature data, we successfully determined shapes and spin states for 55 asteroids that belong to the nominal population of the primitive primordial family of the inner main belt (Delbo' et al. 2017). This corresponds to 51% of the population in the sliver between the left-wing border of the Polana and the primordial family (see Fig. 1). In particular, we calculated 25 new complete asteroid models, 20 revised and 4 new partial models (see Tables B.3 and B.4). Specifically, 34 asteroids have retrograde rotation, while 21 are prograde. The case of (2575) Bulgaria, it is presenting as an example of model fits to the dense and sparse photometric data in Figs. A.2 and A.3, respectively. Fig. A.4 shows an example of four shape models derived from our analysis.

5.3. Identification of interlopers

In order to proceed and study the spin states of the inner main belt primordial family, we need to eliminate any potential interlopers beforehand. As such, are defined the objects that may reside inside the V-shape of a family and/or are grabbed by the HCM methods in the same cluster, but their physical properties, such as their geometric visible albedo p_V and spectral class, are totally different from the bulk composition of the family (Nesvorný et al. 2015). These asteroids that are clearly non-family members, may belong to the background population or to other nearby families.

In our case, seven asteroids have reported spectral (visible or near-infrared) or spectrophotometric (e.g. SDSS, ECAS and MOVIS) data that do not match the primordial family composition, which is composed primarily of dark albedo and featureless spectra. Namely, asteroids (1806) Derice, (2171) Kiev, (2575) Bulgaria and (6125) Singto are classified as S-complex aster-

oids, (2768) Gorky as an A-type, while (5524) Lecacheux and (15415) Rika are classified as V-types in any of the main classification schemes of Tholen (Tholen 1989), Bus (Bus & Binzel 2002) and Bus&DeMeo (DeMeo et al. 2009). Of those, asteroids (1806), (2171), (2575) and (2768) had been already assigned to the nearby bright family of Flora that consists of S-complex asteroid members, a fact that leaves no doubts for them to be interlopers of the low-albedo primordial family of Delbo' et al. (2017). Although asteroids (2536) Kozyrev and (2705) Wu have no spectral or spectrophotometric information their p_V values are moderate and beyond 12% that is generally defined as a separation between the S and C spectroscopic complex (Delbo' et al. 2017). In the studied sample there are seven asteroids (220, 428, 917, 1244, 1544, 1700, 3633) whose p_V is in agreement with the primordial family but are classified as members of the X-complex. Using only the visible part of the spectrum (or spectrophotometric data) is not always sufficient to distinguish the slope between the X and C-complex asteroids, the latter being the main components of the primordial family. So, although these seven asteroids could be indeed interlopers, at this stage we cannot definitely exclude them from the family.

On the other hand, in the population that is studied in this work there are asteroids that had been previously assigned using the clustering methods to the other nearby families of Flora and Vesta (Nesvorný et al. 2015), such as the asteroids (428) Monachia, (4524) Barklajdetolli, (2839) Annette and (3633) Mira. However, their low (<10%) p_V values and their featureless spectrophotometric data are in contrast to this assignment and therefore remain in the primordial family.

This above analysis indicated 9 interlopers in the sample of 55 studied objects. From these 46 confirmed asteroid members of the primordial family, 31 asteroid (67%) models have retrograde rotation and 15 prograde, including also the partial solutions. Excluding the seven X-complex asteroids the abundance of retrograde asteroid reaches 72%. The distribution of the sense of rotation (i.e., prograde or retrograde) within the family is presented in Fig. 1 (Panel B). Additionally, Fig. 2 illustrates the distribution of spin axis directions. Table 1 presents all the objects studied in this work, indicating their prograde or retrograde spin, along with their physical properties. Diameters (D) and geometric albedos (p_V) were calculated as the weighted averages of all the available measurements in the literature and were retrieved from the Minor Planet Physical Properties Catalogue. All uncertainty-weighted averages use $1/\sigma^2$ as weights, where σ is the error of each measurement.

6. Discussion

6.1. The cases of (2171) Kiev, (7132) Casuli and (2705) Wu

The majority of asteroids, studied in our sample are found to be single objects with no evidence of any close-companion body or satellite. However, two asteroids in our sample host a satellite, while another probably is a non-principal-axis (NPA) rotator.

The first two cases are (2171) Kiev and (7132) Casuli, which have been reported as binaries by Loera-González et al. (2020) and Franco et al. (2020a), respectively. Our dense photometric data confirm that (2171) Kiev and (7132) Casuli are indeed binary asteroids, however the observed lightcurves are not enough to provide further constrain of their secondary's orbit. In each case, the eclipsing part of the lightcurve was removed and the CI method was applied on the rotational lightcurves of the primary body. Thus, the results presented in Tables. 1 and B.3 concern only the primary bodies. Although the derived parameters do not deviate from the rest of the sample, one has to be cautious that the companion body can alter the spin axis and rotational characteristics of the primary body.

The third case, (2705) Wu, is a slow retrograde rotator, as the analysis of Ďurech et al. (2020) and ours has shown by using sparse photometric data. Previous dense-in-time observations have shown that is possibly a NPA rotator (i.e. tumbler, Oey 2010). As it has been noted, some deviations from the single periodicity are clearly seen but not at a conclusive level, while more photometric data are needed to resolve the second period. In this study, no further dense-in-time observations were obtained. The characteristic timescale of damping of the excited NPA rotation can be estimated as: $\tau_d = P^3_{[h]}/(C^3 \cdot D^2_{[km]})$ [Gyr] by Harris (1994), where $C = 17 \pm 2.5$ Gyr $\cdot$ km^2/h^3. For this asteroid, the damping timescale is estimated to be 12 ± 5 Gyr, which is greater than the age of our Solar System. This is something statistically common for NPAs, which have diameter larger than $\sim$ 0.4 km (Pravec et al. 2005). So, if (2705) Wu is a tumbler, the spin solution of our study remain trustful concerning the sense of rotation.

6.2. Distribution of the spin poles

All asteroid models with retrograde solutions, except the solutions for (933) Susi and (49863) 1999 XK104, have large ecliptic pole latitude values $|\beta| \geq 30^\circ$ with a large predominance towards the YORP end state values approaching $\beta \sim -90^\circ$. The latitude distribution for prograde rotators differs slightly from the retrograde ones by having more values with $|\beta| \leq 60^\circ$. This is likely due to various resonances acting only on prograde rotators. Similar behavior is also observed in other asteroid families (Hanuš et al. 2013a).

The distribution of ecliptic pole longitudes is bi-modal for prograde rotators with two peaks (at $\sim 45^\circ$ and $\sim 225^\circ$) and irregular (with two peaks at $\sim 75^\circ$ and $\sim 255^\circ$) for retrograde asteroids. Previous studies have estimated that the longitude distribution for main belt asteroids is uniform with no statistically significant features (Kryszczyńska et al. 2007; Hanuš et al. 2011). On the contrary, more recent studies present an anisotropic longitude distribution with two symmetrical maxima around $\sim 50^\circ$ and $\sim 230^\circ$ and minima around $\sim 140^\circ$ and $\sim 320^\circ$ (Bowell et al. 2014; Cibulková et al. 2016).

Retrograde and prograde asteroids have also different period distributions. As Fig. 3 shows, the majority of slow rotators are retrograde. Moreover, the periods of retrograde asteroids have a non-Maxwellian distribution with excesses both at the fast and slow rotations. This bimodal distribution is in agreement with that of main belt asteroids <40 km, as a result of the YORP effect (Pravec & Harris 2000; Pravec et al. 2002). The period distribution of prograde asteroids have an irregular distribution with small peaks for slow, moderate and fast rotations. Thus, prograde and retrograde seems to have different spin rate distributions. A simple model by Pravec et al. (2008) estimated that a uniform distribution for <40 km main belt asteroids could happen on large timescales. Moreover, the different spin rate distributions could signify a different YORP evolution (Pravec & Harris 2000; Pravec et al. 2002, 2008, and references therein).

6.3. The statistical predominance of the retrograde spin poles

It is possible to test if the observed predominance of the retrograde spin poles could be due to chance, i.e., created by random sampling an equal-probability population of prograde and retro-

Table 1. Physical properties of asteroids of the inner main belt primordial family presented in this study, where D and p_V the diameter and the geometric visible albedo respectively. These values are retrieved from the Minor Planet Physical Properties Catalogue and represent the uncertainty-weighted average values of each asteroid. Where the spectral classes is known is given with its reference.

Number	Asteroid Name/Designation	D (km)	σD (km)	p_V	σp_V	Spectral Class	Ref.
			Prograde rotators				
249	Ilse	31.57	0.300	0.054	0.0014	Ch	Lazzaro et al. (2004)
428	Monachia	20.55	0.129	0.066	0.0055	X	Alvarez-Candal et al. (2006)
917	Lyka	35.61	0.135	0.043	0.0040	X	Lazzaro et al. (2004)
1216	Askania	10.35	0.086	0.086	0.0075	-	
1544	Vinterhansenia	24.78	0.074	0.049	0.0036	X,D	Carvano et al. (2010); Alvarez-Candal et al. (2006)
1700	Zvezdara	20.54	0.181	0.039	0.0016	X	Zellner et al. (1985)
1806	Derice	10.67	0.060	0.219	0.0512	Sl	Lazzaro et al. (2004)
2171	Kiev	8.30	0.055	0.101	0.0059	S	Avdellidou et al. Sci. Adv. Submitted.
2536	Kozyrev	9.59	0.218	0.195	0.0227	-	
2575	Bulgaria	7.92	0.063	0.270	0.0300	Sr,S	Bus & Binzel (2002); Popescu et al. (2018)
2768	Gorky	10.67	0.085	0.258	0.0367	A	Alvarez-Candal et al. (2006)
4024	Ronan	11.90	0.073	0.055	0.0032	-	
4524	Barklajdetolli	12.62	0.146	0.087	0.0069	U	Popescu et al. (2018)
6125	Singto	6.30	0.479	0.109	0.0382	S	Popescu et al. (2018)
8022	Scottcrossfield	8.51	0.147	0.046	0.0067	C	Carvano et al. (2010)
8315	Bajin	7.44	0.665	0.039	0.0086	-	
9723	Binyang	3.69	0.095	0.117	0.0320	-	
11975	1995 FA1	4.360	1.440	0.060	0.0500	-	
12722	Petrarca	4.52	0.746	0.095	0.0384	C,U	Carvano et al. (2010); Popescu et al. (2018)
30596	Amdeans	5.11	0.158	0.056	0.0074	-	
59072	1998 VV9	4.59	0.070	0.038	0.0045	-	
			Retrograde rotators				
220	Stephania	32.54	0.138	0.060	0.0032	X,Xk	Carvano et al. (2010); Lazzaro et al. (2004)
282	Clorinde	34.01	0.148	0.045	0.0019	B,C	Bus & Binzel (2002); Popescu et al. (2018)
370	Modestia	38.11	0.106	0.059	0.0046	-	
933	Susi	23.42	0.245	0.042	0.0032	C	Carvano et al. (2010); Popescu et al. (2018)
1159	Granada	30.14	0.099	0.046	0.0019	-	
1244	Deira	33.97	0.152	0.046	0.0029	X	Lazzaro et al. (2004)
1705	Tapio	11.81	0.061	0.093	0.0068	B,U	Bus & Binzel (2002); Popescu et al. (2018)
1924	Horus	12.90	0.130	0.070	0.0036	-	
2012	Guo Shou-Jing	11.91	0.076	0.048	0.0016	C	Carvano et al. (2010); Popescu et al. (2018)
2322	Kitt-Peak	11.91	0.085	0.058	0.0060	-	
2705	Wu	7.79	0.319	0.163	0.0330	-	
2772	Dugan	9.58	0.135	0.057	0.0075	B	Bus & Binzel (2002)
2773	Brooks	13.37	0.100	0.042	0.0031	-	
2776	Baikal	13.37	0.100	0.042	0.0031	-	
2778	Tangshan	12.66	0.144	0.062	0.0080	Cb	Bus & Binzel (2002)
2792	Ponomarev	12.52	0.222	0.056	0.0112	-	
2839	Annette	7.44	0.094	0.059	0.0076	-	
3633	Mira	10.09	0.258	0.045	0.0058	X	Carvano et al. (2010)
3684	Berry	9.64	0.495	0.053	0.0096	C	Carvano et al. (2010); Bus & Binzel (2002)
3723	Voznesenskij	9.54	0.029	0.041	0.0015	C	Carvano et al. (2010)
4231	Fireman	17.96	0.557	0.022	0.0014	-	
5081	Sanguin	17.19	0.263	0.056	0.0063	Ch	Bus & Binzel (2002)
5333	Kanaya	13.70	0.035	0.040	0.0011	Ch	Bus & Binzel (2002); Morate et al. (2019)
5524	Lecacheux	19.90	12.770	0.034	0.1020	V	Carvano et al. (2010); Popescu et al. (2018)
5924	Teruo	13.16	0.080	0.059	0.0015	-	
6647	Josse	6.42	0.148	0.049	0.0069	C	Carvano et al. (2010)
13066	1991 PM13	8.60	0.069	0.038	0.0058	B	Popescu et al. (2018)
15415	Rika	2.83	0.488	0.605	0.1924	V	Popescu et al. (2018)
15998	1999 AG2	7.13	0.046	0.087	0.0062	-	
20771	2000 QY150	9.08	0.115	0.047	0.0068	-	
23495	1991 UQ1	7.94	0.088	0.058	0.0054	-	
28736	2000 GE133	7.03	0.680	0.084	0.0186	C	Carvano et al. (2010)
49863	1999 XK104	3.93	0.189	0.054	0.0053	-	
70184	1999 RU3	4.31	0.629	0.137	0.0557	-	

grade asteroids. In particular, we test the probability to obtain 15 or less prograde rotators from 46 observed asteroids, drawing from a population having an equal probability (0.5) to be retrograde and prograde. This is given by Eq. 3:

$$p(\leq 15, 46) = \sum_{j=1}^{15} \binom{46}{j} 0.5^j (1 - 0.5)^{46-j}. \quad (3)$$

Evaluation of Eq. 3 gives $p(\leq 15, 46) = 1.29\%$. This shows that our observations rule out the null hypothesis – that there is no statistical predominance of the retrograde spin poles – at 98.71% probability.

6.4. The YORP reorientation timescale for the primordial family members

Despite a predominance of retrograde spinning asteroids is expected in the inward wing of the V-shape of a collisional family, it is also likely to find prograde rotators. This is because, during the family lifespan of few billions of years, there are a number of processes that can re-orient the spin vector on an asteroid, such as non-catastrophic collisions, activity, or topographic changes due to e.g. mass wasting/movement (see e.g. Paolicchi & Knežević 2016; Bottke et al. 2015, for a discussion). Torques on asteroids due to the unbalanced emitted and reflected radiation (which cause the YORP effect Rubincam 2000) are very sensitive to topographic features, and so are the strength and sign of the YORP effect (the latter can be reversed; Statler 2009). Statler (2009) theoretically showed that YORP is sensitive of small surface features: hence, even a small impact or mass movement could alter the shape sufficiently and change the sense of pole/period evolution. Moreover, as the YORP effect drives some of the family members towards the critical threshold for fast rotation, topographic instability might easily occur, leading to new YORP coefficients, which can drive the spin-pole in the opposite direction. The older a family is the higher is the cumulative probability that some family members may had undergone shape changes or received non-catastrophic impacts, hence the higher the probability to detect prograde rotators in the wing of the V-shape with predominance of retrograde rotators.

Given the above, we used the model of Vokrouhlický et al. (2006) to estimate the evolution of the spin vectors of the family member asteroids. The model of Vokrouhlický et al. (2006) takes into account the change in orbital semimajor axis due to the Yarkovsky effect and the changes in the rotation rate $\frac{d\omega}{dt}$ and spin axis obliquity[11] $\omega\frac{d\epsilon}{dt}$ of the spin axis due to the YORP torques. In particular, the values of $\frac{d\omega}{dt}$ and $\omega\frac{d\epsilon}{dt}$ are multiplied by a constant named C_{YORP}, which Bottke et al. (2015) have proposed to be between 0.5 and 0.7. However, Vokrouhlický et al. (2006) found that values of $C_{YORP} \sim 1$ could produce model asteroid families that well represent the real ones. Hence, we assumed here, for simplicity, $C_{YORP} = 1$. The values of $\frac{d\omega}{dt}$ and $\omega\frac{d\epsilon}{dt}$ are functions of orbital and physical parameters of asteroids, as described by Vokrouhlický et al. (2006), which we follow hereafter.

Following Vokrouhlický et al. (2006), we modelled the evolution of the 46 family members for which we have a pole solution. We assumed they all started with an initial retrograde spin direction, which we randomly assigned uniformly between 90 and 180° obliquity. We initialised model asteroids with the known diameters and current spin periods. We evolved the model

[11] Obliquity (ϵ) is defined as the angle between the equatorial and orbital planes of an asteroid. Note that for small orbital inclination, obliquity of 0° is approximately $\sim 90°$ and 180° is $\sim -90°$, respectively.

with a time step of 10 Myr for 4 Gyr. At each time step, a the values of a, ω, and ϵ were updated by summing their respective time derivatives multiplied by the step in time. At each time step, we also evaluated the probability that an asteroid could suffer a non-catastrophic collision capable of changing its spin axis. This probability is given by the 10 Myr-time step divided by the re-orientation time scale, τ_{reor}, the latter estimated by Eq. 4:

$$\tau_{reor} = 0.845 \left(\frac{5}{P_{[h]}}\right)^{5/6} \left(\frac{D_{[km]}}{2}\right)^{4/3} \quad [Gyr] \tag{4}$$

Then, for each asteroid (an each time step), we extracted a random number, uniformly distributed between 0 and 1, and we re-oriented the spin state of the asteroid when the random number was smaller than said probability. The spin axis re-orientation is performed by picking a new random direction of the obliquity uniformly distributed between 0 and 180°.

After the model was completed, we counted how many of the initially retrograde asteroids became prograde rotators due to spin evolution. We run the model 10,000 times and we found that the probability to have 15 or less prograde rotators of the initially 46 retrograde objects is 13.5%; on average, we find 11.4 prograde asteroids.

However, Delbo' et al. (2017) showed that D≥35 km asteroids could be primordial objects that accreted as planetesimals from the dust of our protoplanetary disk. It is therefore possible that some of these are within the inward wing of the V-shape of the primordial family. Hence, we considered also the aforementioned model only for D<35 asteroids, of which 14 are prograde rotators and 29 retrograde rotators. In this case we found a 20% probability to have 14 or less prograde rotators of the initially 43 retrograde objects is 20%.

We can conclude that it is possible to observe the current mix of retrograde and prograde rotators within the inward wing of the 4 Gyr-old collisional family.

7. Conclusions

We carried out a campaign of photometric observations of those asteroids that have been claimed to be members of one of the oldest collisional (primordial) families in the Solar System (Delbo' et al. 2017). We constructed photometric time series – the lightcurves – for 49 asteroids. This corresponds to 46% of the number of the members of the primordial family. We combined our lightcurves with literature ones and with sparse-in-time photometry in order to create multi-epoch photometric data sets to be used as inputs for the convex inversion method. We obtained 49 new and revised shape models and their spin vector solutions. We combined this with literature spin vectors (6 objects).

We reassessed the albedo values for the observed asteroids and studied their literature spectra. This allowed us to find 9 interlopers among the initial list of family members of Delbo' et al. (2017). After having removed these interlopers, we find that 31 and 15 out of the remaining 46 asteroids are retrograde and prograde, respectively. We show that this predominance of retrograde compared to prograde asteroids is very unlikely (1.29% probability) to be due to sampling a distribution of objects with equal probability to be prograde and retrograde. This corroborates the hypothesis that the statistical predominance of the retrograde spin poles is due to a physical process, as it was claimed by Delbo' et al. (2017), namely formation as collisional fragments of a common parent body, a subsequent dynamical evolution driven by the Yarkovsky effect.

Acknowledgements. MD and CA acknowledge support from ANR "ORIGINS" (ANR-18-CE31-0014). This work is based on data provided by the Minor Planet Physical Properties Catalogue (MP3C) of the Observatoire de la Côte d'Azur. The research of JH has been supported by the Czech Science Foundation through grant 20-08218S. The work of OP has been supported by INTER-EXCELLENCE grant LTAUSA18093 from the Ministry of Education, Youth, and Sports. Support for T.W.-S.H. was provided by NASA through the NASA Hubble Fellowship grant HST-HF2-51458.001-A awarded by the Space Telescope Science Institute (STScI), which is operated by the Association of Universities for Research in Astronomy, Inc., for NASA, under contract NAS5-26555. We thank the Las Cumbres Observatory and their staff for its continuing support of the ASAS-SN project. ASAS-SN is supported by the Gordon and Betty Moore Foundation through grant GBMF5490 to the Ohio State University, and funded in part by the Alfred P. Sloan Foundation grant G-2021-14192 and NSF grant AST-1908570. Development of ASAS-SN has been supported by NSF grant AST-0908816, the Mt. Cuba Astronomical Foundation, the Center for Cosmology and AstroParticle Physics at the Ohio State University, the Chinese Academy of Sciences South America Center for Astronomy (CAS-SACA), the Villum Foundation, and George Skestos.

References

Alvarez-Candal, A., Duffard, R., Lazzaro, D., & Michtchenko, T. 2006, A&A, 459, 969
Athanasopoulos, D., Bonamico, R., Van Belle, G., et al. 2021, in European Planetary Science Congress Vol. 15, EPSC2021–335
Baker, R. E., Benishek, V., Pilcher, F., & Higgins, D. 2010, Minor Planet Bulletin, 37, 81
Bellm, E. C., Kulkarni, S. R., Graham, M. J., et al. 2019, PASP, 131, 018002
Bendjoya, P., Abe, L., Rivet, J. P., et al. 2012, in SF2A-2012: Proceedings of the Annual meeting of the French Society of Astronomy and Astrophysics, ed. S. Boissier, P. de Laverny, N. Nardetto, R. Samadi, D. Valls-Gabaud, & H. Wozniak, 643–648
Benishek, V. 2017, Minor Planet Bulletin, 44, 67
Benishek, V. 2020, Minor Planet Bulletin, 47, 75
Berry, R. & Burnell, J. 2005, The handbook of astronomical image processing, Vol. 2
Berthier, J., Hestroffer, D., Carry, B., et al. 2009, in European Planetary Science Congress 2009, 676
Binzel, R. P. 1987, Icarus, 72, 135
Binzel, R. P. & Mulholland, J. D. 1983, Icarus, 56, 519
Binzel, R. P., Xu, S., Bus, S. J., & Bowell, E. 1992, Icarus, 99, 225
Bolin, B. T., Delbo, M., Morbidelli, A., & Walsh, K. J. 2017, Icarus, 282, 290
Bonamico, R. & van Belle, G. 2021, Minor Planet Bulletin, 48, 210
Bottke, W. F., Vokrouhlický, D., Walsh, K. J., et al. 2015, Icarus, 247, 191
Bowell, E., Oszkiewicz, D. A., Wasserman, L. H., et al. 2014, Meteoritics and Planetary Science, 49, 95
Broeg, C., Fernández, M., & Neuhäuser, R. 2005, Astronomische Nachrichten, 326, 134
Brož, M. & Morbidelli, A. 2013, Icarus, 223, 844
Buchheim, R. K. 2007, Minor Planet Bulletin, 34, 68
Bus, S. J. & Binzel, R. P. 2002, Icarus, 158, 146
Carreño, A., Arce, E., Fornas, G., & Mas, V. 2019, Minor Planet Bulletin, 46, 200
Carvano, J. M., Hasselmann, P. H., Lazzaro, D., & Mothé-Diniz, T. 2010, A&A, 510, A43
Chang, C.-K., Ip, W.-H., Lin, H.-W., et al. 2015, ApJS, 219, 27
Cibulková, H., Ďurech, J., Vokrouhlický, D., Kaasalainen, M., & Oszkiewicz, D. A. 2016, A&A, 596, A57
Cooney, W., Benishek, V., Pravec, P., et al. 2017, Central Bureau Electronic Telegrams, 4401, 1
Deienno, R., Walsh, K. J., & Delbo, M. 2021, Icarus, 357, 114218
Delbo, M., Avdellidou, C., & Morbidelli, A. 2019, A&A, 624, A69
Delbo', M., Walsh, K., Bolin, B., Avdellidou, C., & Morbidelli, A. 2017, Science, 357, 1026
DeMeo, F. E., Binzel, R. P., Slivan, S. M., & Bus, S. J. 2009, Icarus, 202, 160
Dermott, S. F., Li, D., Christou, A. A., et al. 2021, MNRAS, 505, 1917
Ďurech, J., Hanuš, J., Oszkiewicz, D., & Vančo, R. 2016, A&A, 587, A48
Ďurech, J., Hanuš, J., & Alí-Lagoa, V. 2018a, A&A, 617, A57
Ďurech, J., Hanuš, J., Brož, M., et al. 2018b, Icarus, 304, 101
Ďurech, J., Hanuš, J., & Vančo, R. 2019, A&A, 631, A2
Ďurech, J., Kaasalainen, M., Warner, B. D., et al. 2009, A&A, 493, 291
Durech, J., Sidorin, V., & Kaasalainen, M. 2010, A&A, 513, A46
Erasmus, N., Kramer, D., McNeill, A., et al. 2021, MNRAS, 506, 3872
Erasmus, N., Navarro-Meza, S., McNeill, A., et al. 2020, ApJS, 247, 13
Fauvaud, S. & Fauvaud, M. 2013, Minor Planet Bulletin, 40, 224
Fauvaud, S. & Fauvaud, M. 2014, Minor Planet Bulletin, 41, 143

Ferrero, A. 2021, Minor Planet Bulletin, 48, 215
Franco, L., Marchini, A., Bonnoli, G., et al. 2020a, The Astronomer's Telegram, 13590, 1
Franco, L., Marchini, A., Saya, L.-F., et al. 2020b, Minor Planet Bulletin, 47, 242
Gaia Collaboration, Spoto, F., Tanga, P., et al. 2018, A&A, 616, A13
Gallaway, M. 2020, in An Introduction to Observational Astrophysics (Springer), 169–181
Gazeas, K. 2016, in Revista Mexicana de Astronomia y Astrofisica Conference Series, Vol. 48, 22–23
Goudis, C., Hantzios, P., Boumis, P., et al. 2010, in Astronomical Society of the Pacific Conference Series, Vol. 424, 9th International Conference of the Hellenic Astronomical Society, ed. K. Tsinganos, D. Hatzidimitriou, & T. Matsakos, 422
Hanuš, J., Brož, M., Ďurech, J., et al. 2013a, A&A, 559, A134
Hanuš, J., Delbo', M., Alí-Lagoa, V., et al. 2018, Icarus, 299, 84
Hanuš, J., Ďurech, J., Brož, M., et al. 2013b, A&A, 551, A67
Hanuš, J., Ďurech, J., Brož, M., et al. 2011, A&A, 530, A134
Hanuš, J., Ďurech, J., Oszkiewicz, D. A., et al. 2016, A&A, 586, A108
Hanuš, J., Pejcha, O., Shappee, B. J., et al. 2021, A&A, 654, A48
Harris, A. W. 1994, Icarus, 107, 209
Higgins, D. 2008, Minor Planet Bulletin, 35, 30
Higgins, D. 2011, Minor Planet Bulletin, 38, 41
Hirayama, K. 1918, AJ, 31, 185
Kaasalainen, M. & Lamberg, L. 2006, Inverse Problems, 22, 749
Kaasalainen, M., Mottola, S., & Fulchignoni, M. 2002, in Asteroids III, 139–150
Kaasalainen, M. & Torppa, J. 2001, Icarus, 153, 24
Kaasalainen, M., Torppa, J., & Muinonen, K. 2001, Icarus, 153, 37
Klinglesmith, Daniel A., I. 2017, Minor Planet Bulletin, 44, 127
Kochanek, C. S., Shappee, B. J., Stanek, K. Z., et al. 2017, PASP, 129, 104502
Kryszczyńska, A., Colas, F., Polińska, M., et al. 2012, A&A, 546, A72
Kryszczyńska, A., La Spina, A., Paolicchi, P., et al. 2007, Icarus, 192, 223
Lagerkvist, C. I. & Magnusson, P. 2011, NASA Planetary Data System, EAR
Larson, S., Beshore, E., Hill, R., et al. 2003, in Bulletin of the American Astronomical Society, Vol. 35, AAS/Division for Planetary Sciences Meeting Abstracts #35, 982
Lazzaro, D., Angeli, C. A., Carvano, J. M., et al. 2004, Icarus, 172, 179
Loera-González, P., Olguín, L., Saucedo-Morales, J., & Nuñez-López, R. 2020, Minor Planet Bulletin, 47, 348
Lumme, K. & Bowell, E. 1981, AJ, 86, 1705
Mahlke, M., Carry, B., & Denneau, L. 2021, Icarus, 354, 114094
Masiero, J. R., Carruba, V., Mainzer, A., Bauer, J. M., & Nugent, C. 2015, ApJ, 809, 179
Massey, P. 1997, National Optical Astronomy Observatory
Milani, A., Cellino, A., Knežević, Z., et al. 2014, Icarus, 239, 46
Millis, R. L., Bowell, E., & Thompson, D. T. 1976, Icarus, 28, 53
Mohamed, R. A., Chiorny, V. G., Dovgopol, A. N., & Shevchenko, V. G. 1994, A&AS, 108, 69
Morate, D., de León, J., De Prá, M., et al. 2019, A&A, 630, A141
Nesvorný, D., Brož, M., & Carruba, V. 2015, Identification and Dynamical Properties of Asteroid Families, ed. P. Michel, F. E. DeMeo, & W. F. Bottke, 297–321
Oey, J. 2010, Minor Planet Bulletin, 37, 53
Pál, A., Szakáts, R., Kiss, C., et al. 2020, ApJS, 247, 26
Paolicchi, P. & Knežević, Z. 2016, Icarus, 274, 314
Pilcher, F. 2015, Minor Planet Bulletin, 42, 190
Polakis, T. 2021, Minor Planet Bulletin, 48, 158
Popescu, M., Licandro, J., Carvano, J. M., et al. 2018, A&A, 617, A12
Pravec, P. & Harris, A. W. 2000, Icarus, 148, 12
Pravec, P., Harris, A. W., & Michalowski, T. 2002, in Asteroids III, 113–122
Pravec, P., Harris, A. W., Scheirich, P., et al. 2005, Icarus, 173, 108
Pravec, P., Harris, A. W., Vokrouhlický, D., et al. 2008, Icarus, 197, 497
Pray, D. P. & Durkee, R. I. 2010, Minor Planet Bulletin, 37, 35
Ricker, G. R., Winn, J. N., Vanderspek, R., et al. 2015, Journal of Astronomical Telescopes, Instruments, and Systems, 1, 014003
Rubincam, D. P. 2000, Icarus, 148, 2
Shappee, B. J., Prieto, J. L., Grupe, D., et al. 2014, ApJ, 788, 48
Skiff, B. A., McLelland, K. P., Sanborn, J. J., Pravec, P., & Koehn, B. W. 2019, Minor Planet Bulletin, 46, 238
Statler, T. S. 2009, Icarus, 202, 502
Stephens, R. & Warner, B. D. 2018, in AAS/Division for Planetary Sciences Meeting Abstracts, Vol. 50, AAS/Division for Planetary Sciences Meeting Abstracts #50, 417.03
Stephens, R. D. 2011, Minor Planet Bulletin, 38, 23
Stephens, R. D. & Warner, B. D. 2010, Minor Planet Bulletin, 37, 124
Stephens, R. D. & Warner, B. D. 2019a, Minor Planet Bulletin, 46, 389
Stephens, R. D. & Warner, B. D. 2019b, Minor Planet Bulletin, 46, 449
Stephens, R. D. & Warner, B. D. 2020, Minor Planet Bulletin, 47, 224
Strabla, L., Quadri, U., & Girelli, R. 2011, Minor Planet Bulletin, 38, 169
Tholen, D. J. 1989, in Asteroids II, ed. R. P. Binzel, T. Gehrels, & M. S. Matthews (University of Arizona Press), 1139–1150
Tonry, J. L., Denneau, L., Heinze, A. N., et al. 2018, PASP, 130, 064505
Tsirvoulis, G., Morbidelli, A., Delbo, M., & Tsiganis, K. 2018, Icarus, 304, 14
Ďurech, J., Tonry, J., Erasmus, N., et al. 2020, A&A, 643, A59
Vokrouhlický, D., Bottke, W. F., Chesley, S. R., Scheeres, D. J., & Statler, T. S. 2015, in Asteroids IV, ed. P. Michel, F. E. DeMeo, & W. F. Bottke (The University of Arizona Press), 509–531
Vokrouhlický, D., Brož, M., Bottke, W. F., Nesvorný, D., & Morbidelli, A. 2006, Icarus, 182, 118
Walsh, K. J., Delbó, M., Bottke, W. F., Vokrouhlický, D., & Lauretta, D. S. 2013, Icarus, 225, 283
Warner, B. D. 2004, Minor Planet Bulletin, 31, 36
Warner, B. D. 2006, Minor Planet Bulletin, 33, 58
Warner, B. D. 2010, Minor Planet Bulletin, 37, 161
Warner, B. D. 2014, Minor Planet Bulletin, 41, 144
Warner, B. D., Harris, A. W., & Pravec, P. 2009, Icarus, 202, 134
Warner, B., D. 2015, MPO Canopus software
Waszczak, A., Chang, C.-K., Ofek, E. O., et al. 2015, AJ, 150, 75
Wisniewski, W. Z., Michałowski, T. M., Harris, A. W., & McMillan, R. S. 1997, Icarus, 126, 395
Zappala, V., Bendjoya, P., Cellino, A., Farinella, P., & Froeschlé, C. 1995, Icarus, 116, 291
Zappala, V., Cellino, A., Farinella, P., & Knezevic, Z. 1990, AJ, 100, 2030
Zellner, B., Tholen, D. J., & Tedesco, E. F. 1985, Icarus, 61, 355

[1] Section of Astrophysics, Astronomy and Mechanics, Department of Physics, National and Kapodistrian University of Athens, Zografos GR 15784, Athens, Greece
e-mail: dimathanaso@phys.uoa.gr
[2] Charles University, Faculty of Mathematics and Physics, Institute of Astronomy, V Holešovičkách 2, CZ-18000, Prague 8, Czech Republic
e-mail: josef.hanus@mff.cuni.cz
[3] Université Côte d'Azur, Observatoire de la Côte d'Azur, CNRS, Laboratoire LAGRANGE, France
[4] BSA Osservatorio (K76), Strada Collarelle 53, 12038 Savigliano, Cuneo, Italy
[5] Bigmuskie Observatory (B88), via Italo Aresca 12, 14047 Moberelli, Asti, Italy
[6] NOAK Observatory (L02), Stavraki Ioannina, Greece
[7] Lowell Observatory, 1400 West Mars Hill Road, Flagstaff, AZ 86001, USA
[8] Observatoire des Hauts Patys, F-84410 Bédoin, France
[9] Observatoire de Chinon, Mairie de Chinon, 37500 Chinon, France
[10] Geneva Observatory, CH-1290 Sauverny, Switzerland
[11] Observatoire des Engarouines, 1606 chemin de Rigoy, F-84570 Malemort-du-Comtat, France
[12] Via Capote Observatory, Thousand Oaks, CA 91320, USA
[13] AstroQueyras, 05530 Saint-Véran, France
[14] Le Florian, Villa 4, 880 chemin de Ribac-Estagnol, F-06600 Antibes, France
[15] Observatoire du Bois de Bardon, 16110 Taponnat, France
[16] Courbes de rotation d'astéroïdes et de comètes
[17] Hunters Hill Observatory, 7 Mawalan Street, Ngunnawal ACT 2913, Australia
[18] NHFP Einstein Fellow
[19] The Observatories of the Carnegie Institution for Science, 813 Santa Barbara St., Pasadena, CA 91101, USA
[20] Courbes de rotation d'astéroïdes et de comètes
[21] Antelope Hills Observatory, 980 Antelope DR W, Bennett, CO 80102 USA
[22] Astronomical Observatory Institute, Faculty of Physics, A. Mickiewicz University, Słoneczna 36, 60-286 Poznań, Poland
[23] Innstitut d'Astrophysique de Paris, 98 bis boulevard Arago, UMR 7095 CNRS et Sorbonne Universités, 75014 Paris, France
[24] Blue Mountains Observatory, Leura, Australia
[25] Charles University, Faculty of Mathematics and Physics, Institute of Theoretical Physics, V Holešovičkách 2, 18000 Prague, Czech Republic
[26] Observatoire de Blauvac, 293 chemin de St Guillaume, F-84570 77 Blauvac, France

Appendix A: Supplementary figures

Appendix B: Supplementary tables

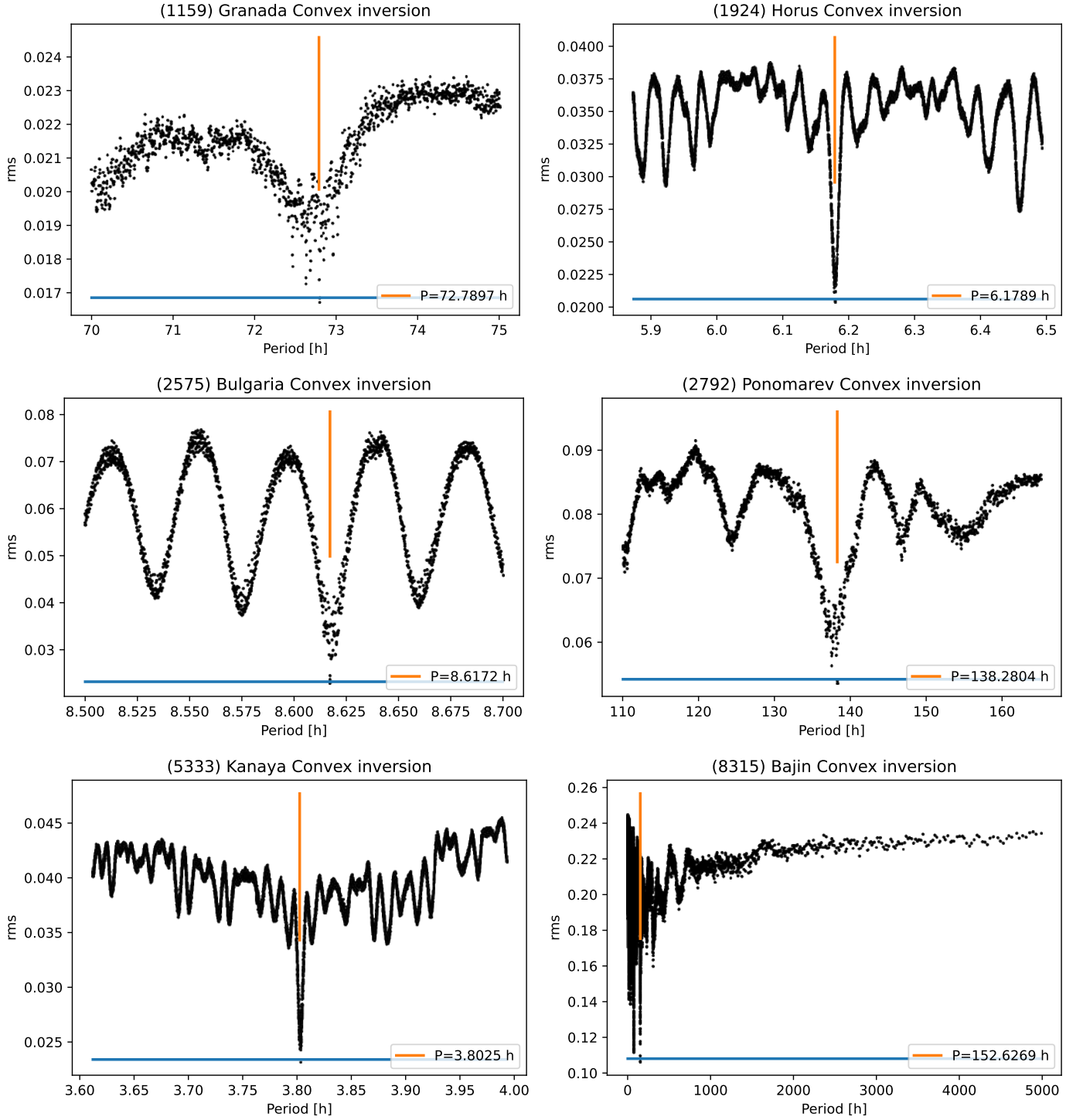

Fig. A.1. Example of typical periodograms of six different asteroids for which we present their new shape model determinations. Each dot represents one trial run sampling all the local minima at fixed rotation period (Eq. 2) within the searched interval. The vertical lines indicate the best-fitting values. The horizontal line represents the χ^2 threshold defined by Eq. 1.

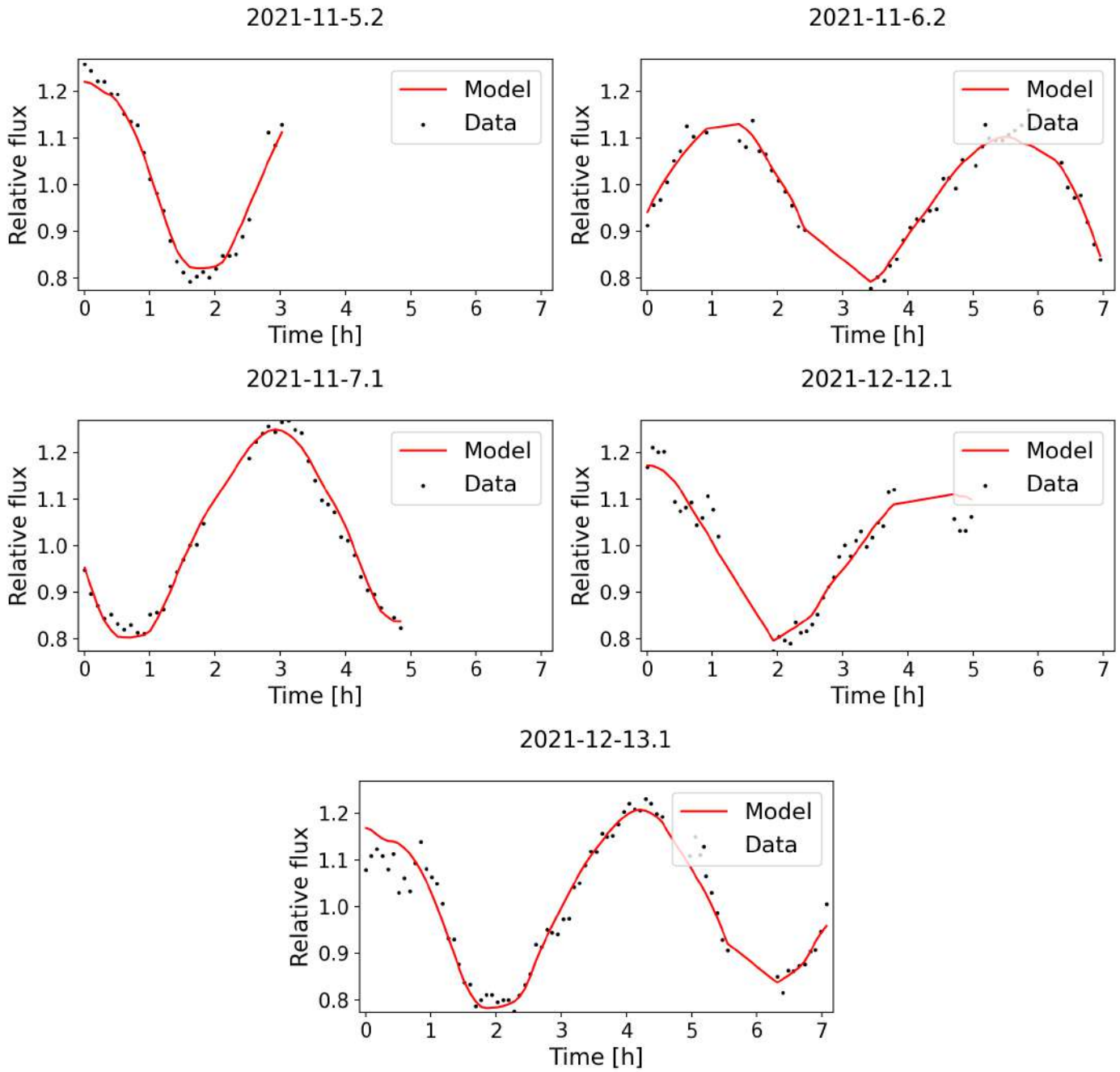

Fig. A.2. Example of fits to the dense light curves for asteroid (2575) Bulgaria. All five light curves were obtained in the framework of this study (observed Andrea Ferrero).

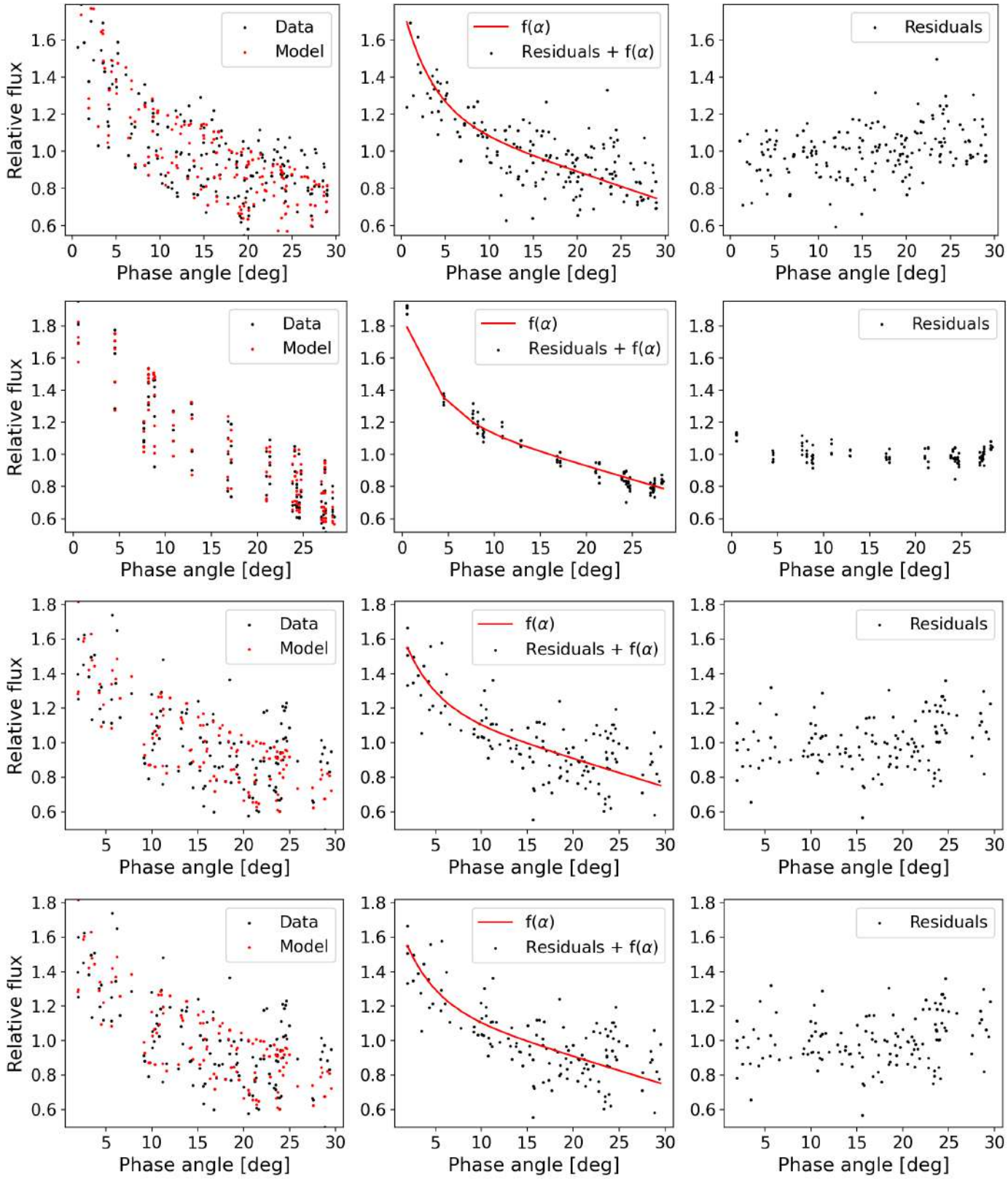

Fig. A.3. Example of fits to the sparse data sets for asteroid (2575) Bulgaria. The function f(α) is a semi-empirical phase function (Kaasalainen et al. 2002) that we fit. The data sets are as follows (top to bottom): ASAS-SN *V*-band, ASAS-SN *g*-band, ATLAS *c*-band, and ATLAS *o*-band.

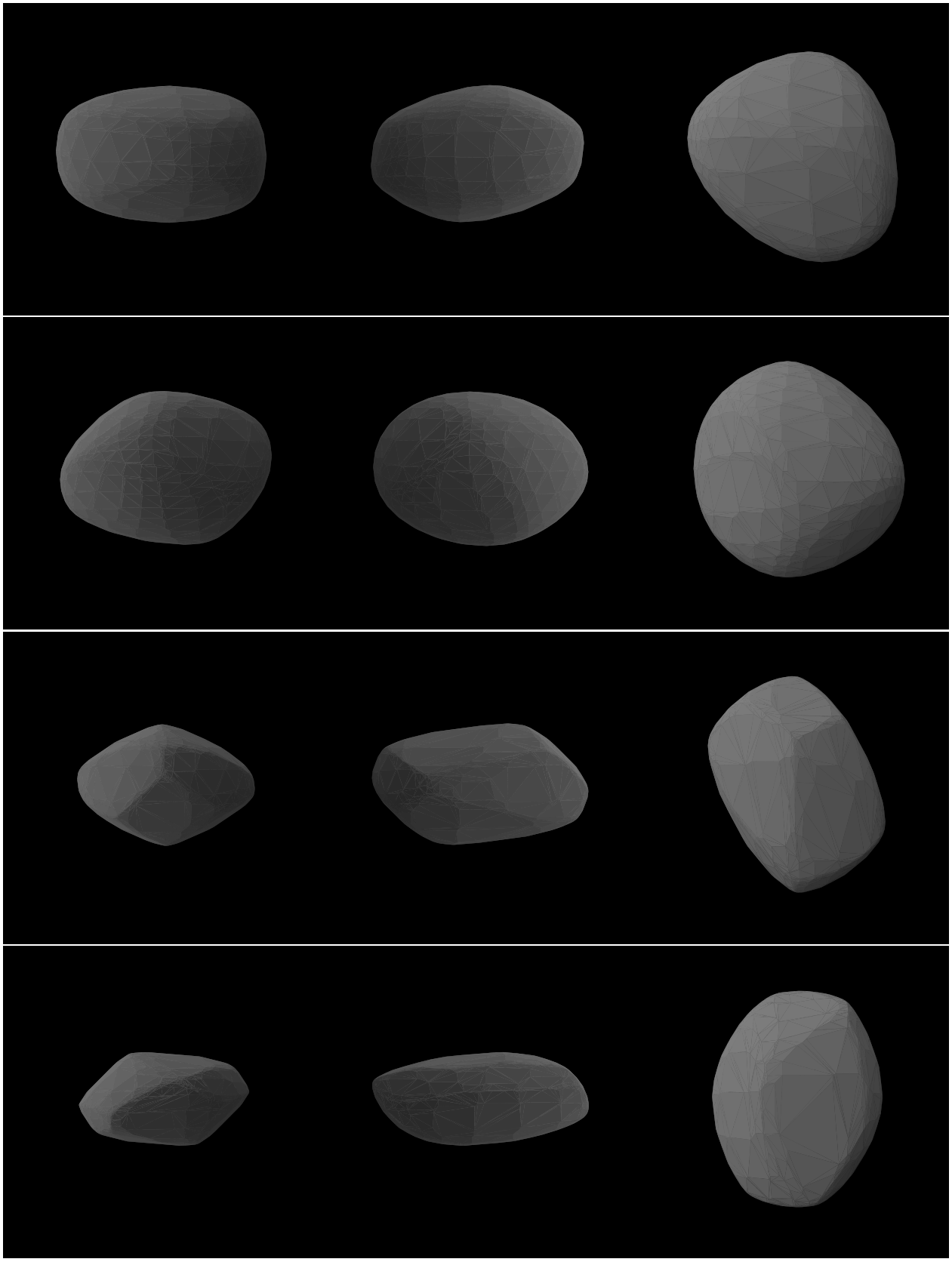

Fig. A.4. Example of several shape models. The first the view are equatorial with a 90° rotation offset and the third one is north pole-on. We always show the first pole solution and the asteroids are as follows (top to bottom): (1159) Granada, (1700) Zvezdara, (2575) Bulgaria, and (2792) Ponomarev.

Table B.1. Asteroids which spin poles are known from the literature, where P is the sidereal period and λ, β, the ecliptic longitude and latitude of the spin axis respectively.

Asteroid		P	λ_1	β_1	λ_2	β_2	Original model
Number	Name/Designation	(h)	(deg)	(deg)	(deg)	(deg)	publication
220	Stephania	18.209	26	−50	223	−62	Hanuš et al. (2013b)
249	Ilse	84.995	2	85	222	41	Hanuš et al. (2016)
282	Clorinde	49.36	353	−66	184	−47	Ďurech et al. (2020)
370	Modestia	22.5411	–	−50 ± 9	–	–	Ďurech et al. (2020)
428	Monachia	3.63360	–	51 ± 9	–	–	Ďurech et al. (2020)
933	Susi	4.6224	301	−10	125	−15	Ďurech et al. (2020)
1216	Askania	6.53713	–	44 ± 14	–	–	Ďurech et al. (2020)
1244	Deira	216.98	107	−56	314	−46	Hanuš et al. (2016)
1705	Tapio	25.544	265	−48	106	−57	Ďurech et al. (2018a)
2012	Guo Shou−Jing	228.33	–	−59 ± 18	–	–	Ďurech et al. (2020)
2536	Kozyrev	7.189	257	16	79	18	Ďurech et al. (2020)
2705	Wu	150.8	356	−81	138	−55	Ďurech et al. (2020)
2772	Dugan	235.72	–	−58 ± 20	–	–	Ďurech et al. (2020)
2839	Annette	10.4609	154	−36	341	−49	Hanuš et al. (2013b)
4231	Fireman	339.5	72	−43	258	−36	Ďurech et al. (2019)
4524	Barklajdetolli	965.9	–	49 ± 16	–	–	Ďurech et al. (2020)
5081	Sanguin	10.26460	–	−49 ± 5	–	–	Ďurech et al. (2020)
5524	Lecacheux	8.41706	–	−57 ± 9	–	–	Ďurech et al. (2020)
5924	Teruo	9.9918	340	−44	164	−34	Ďurech et al. (2019)
6125	Singto	10.2642	–	43 ± 17	–	–	Ďurech et al. (2020)
9723	Binyang	12.388	–	55 ± 2	–	–	Ďurech et al. (2018a)
20771	2000 QY150	8.3014	4	−47	172	−48	Ďurech et al. (2019)
28736	2000 GE133	4.6544	249	−52	134	−84	Hanuš et al. (2016)
30596	Amdeans	23.134	114	35	294	37	Ďurech et al. (2018a)
59072	1998 VV9	7.2982	41	40	223	30	Ďurech et al. (2018a)

Table B.2. Photometric observations of targets in the frame of *Ancient Asteroids* campaign. The literature value of the (synodic) rotational period is given, along with the observing log, where N_{LC} is the number of individual lightcurves, obtained by each corresponding observing site given in the last column, while N_{app} is the number of apparitions. The standard error for each value is expressed in parentheses, in units of last decimal digit quoted.

Asteroid Number	Asteroid Name/Designation	$P_{synodic}$ (h)	Observing season	N_{LC}	N_{app}	Site*
282	Clorinde	49.352(4)[a]	Nov 2020 - Mar 2021	7+20	1	BSA+Lowell
370	Modestia	22.5299(1)[c]	Aug 2021 - Oct 2021	6+1	1	NOAK+OBdB
428	Monachia	3.6343(5)[b]	Mar 2018	1	1	BE600
853	Nansenia	7.931(2)[d]	Dec 2020 - Mar 2021	15	1	Lowell
933	Susi	4.6222(4)[f]	Feb 2018 - Jan 2021	3+5+1	2	BSA+Lowell+BE600
1159	Granada	77.28(5)[d]	Oct 2021	1+2	1	C2PU+UOAO
1700	Zvezdara	9.098(2)[d]	Nov 2020 - Jan 2021	2+11	1	BSA+Lowell
1806	Derice	3.22443(1)[g]	May 2021	3	1	BSA
1924	Horus	6.177(14)[h]	Sep 2021 - Nov 2021	6	1	BO
2012	Guo Shou-Jing	–	Oct 2021 - Dec 2021	15	1	BO
2171	Kiev	3.1714(2)[b]	Jan 2022	3	1	BO
2259	Sofievka	63.0918(5)[b]	Dec 2020 - Jan 2021	9	1	BSA
2322	Kitt-Peak	8.460(6)[j]	Nov 2020 - Jan 2021	4+9	1	BSA+Lowell
2575	Bulgaria	8.618(7)[k]	Nov 2021 - Dec 2021	5	1	BO
2768	Gorky	4.5118(7)[d]	Dec 2019 - May 2021	4+3+9	2	BSA+BO+UOAO
2772	Dugan	235.0(5)[f]	Dec 2007	1	1	BMO
2773	Brooks	4.838(1)[d]	Sep 2021 - Oct 2021	4	1	BSA
2776	Baikal	–	Jan 2007	1	1	BMO
2778	Tangshan	3.468(3)[l]	Nov 2020 - Oct 2021	3+6	1	BSA+Lowell
2839	Annette	10.459(5)[b]	Apr 2020	5	1	UOAO
3633	Mira	19.17(2)[h]	Nov 2021 - Jan 2022	12	1	BO
3723	Voznesenskij	7.9640(85)[h]	Oct 2021	2+1	1	C2PU+Helmos
4231	Fireman	28.0(2)[d]	Dec 2020 - Apr 2021	19	1	Lowell
4422	Jarre	7.013(1)[m]	Apr 2021 - May 2021	5+3+9+3	1	BSA+Lowell+BO+UOAO
5081	Sanguin	10.2619(5)[b]	May 2021 - Jun 2021	6	1	BSA
5333	Kanaya	3.69(5)[d]	Jun 2021 - Jul 2021	3+1	1	C2PU+ChR
6125	Singto	10.2642(1)[b]	Jan 2022	3	1	BO
7132	Casulli	3.5238(2)[n]	Oct 2021	3+1	1	C2PU+Helmos
9086	1995 SA3	–	Oct 2019 - Nov 2019	22	1	UOAO
9972	Minoruoda	3.4221(2)[o]	Oct 2021	1	1	Helmos
10542	Ruckers	–	Feb 2022 - Mar 2022	4	1	BO
15985	1998 WU20	18.2252(5)[b]	Oct 2021	4+1	1	C2PU+Helmos
25343	1999 RA44	590.5(5)[m]	Jan 2021 - Apr 2021	27	1	BO

Notes. [*] BSA:Astronomical Observatory BSA, Lowell: Lowell Observatory, BO: Bigmuskie Observatory, C2PU: Observatoire de la Côte d'Azur (OCA) - Calern station, UOAO: University of Athens Observatory, Helmos: Helmos Observatory of National Observatory of Athens, NOAK: NOAK Observatory, BE600: BlueEye 600 Observatory, ChR: Pic de Château-Renard Observatory, OBdB: Observatoire du Bois de Bardon, BMO:Blue Mountains Observatory
[a] Bonamico & van Belle (2021) , [b] Pál et al. (2020) , [c] Stephens (2011) , [d] `http://obswww.unige.ch/~behrend/page_cou.html` , [f] `https://www.asu.cas.cz/~ppravec/` , [f] `https://web.archive.org/web/20081004205615/http://www.david-higgins.com/` , [g] Stephens & Warner (2020) , [h] Waszczak et al. (2015) , [i] Mahlke et al. (2021) , [j] Polakis (2021) , [k] Erasmus et al. (2020) , [l] Stephens & Warner (2019b) , [m] Ferrero (2021) , [n] Franco et al. (2020b) , [o] Cooney et al. (2017)

Table B.3. Rotation state properties and summary of the optical dataset for asteroids for which we derived new shape solution or estimated their sense of rotation.

Number	Asteroid Name/Designation	λ_1 (deg)	β_1 (deg)	λ_2 (deg)	β_2 (deg)	P (h)	N_{LC}	N_{app}	N_{689}	N_{703}	N_{GAI}	N_{ASA}	N_{ATL}	N_{I41}	N_{PTF}
New asteroid models															
917	Lyka	44	49	230	37	7.88167	13	1	116	205	9	599	582	26	0
1159	Granada	70	−54	142	−85	72.789	5	2	130	196	14	382	508	77	49
1544	Vinterhansenia	55	22	238	23	13.78270	0	0	104	215	9	389	341	0	0
1700	Zvezdara	66	62	248	48	9.11217	43	2	116	176	20	354	324	51	0
1806	Derice	42	43	216	38	3.223531	17	2	59	286	0	406	488	20	0
1924	Horus	131	−59	315	−54	6.17893	6	1	0	178	0	163	459	29	21
2171	Kiev	145	54			3.171587	7	2	0	277	12	339	451	0	0
2322	KittPeak	195	−78			8.46780	13	1	0	191	0	319	425	0	0
2575	Bulgaria	66	91	246	70	8.61720	5	1	20	205	0	309	445	0	28
2768	Gorky	54	34			4.50814	18	2	37	217	11	151	545	0	0
2773	Brooks	85	−86	241	−71	4.83726	7	2	0	162	14	110	328	0	0
2776	Baikal	81	−41	264	−27	3253.5	1	1	0	143	0	312	479	44	0
2792	Ponomarev	72	−58	230	−82	138.28	0	0	0	193	0	223	409	92	60
3633	Mira	170	−58	346	−50	19.1832	12	1	0	275	10	124	331	0	29
3684	Berry	96	−57	255	−49	11.9074	0	0	0	186	0	0	332	0	0
3723	Voznesenskij	75	−35	259	−34	7.96485	3	1	0	185	0	52	292	0	20
5333	Kanaya	157	−56			3.80247	9	2	0	172	25	210	533	0	0
6647	Josse	38	−68	222	−62	5.94972	6	1	0	165	0	24	271	0	0
8022	Scottcrossfield	186	30	359	40	4.00267	0	0	0	228	18	84	293	0	76
8315	Bajin	6	71			152.62	0	0	0	167	0	0	262	74	0
12722	Petrarca	143	24	346	41	3.538576	0	0	0	138	0	0	175	41	0
15415	Rika	117	−79			6.36228	0	0	0	164	0	0	275	0	0
23495	1991 UQ1	84	−70			10.50559	0	0	0	124	0	26	370	0	0
49863	1999 XK104	32	−18	212	−22	8.00795	0	0	0	72	0	0	94	0	0
Number	Asteroid Name/Designation	β_P (deg)	$\delta\beta$ (deg)			P (h)	N_{LC}	N_{app}	N_{689}	N_{703}	N_{GAI}	N_{ASA}	N_{ATL}	N_{I41}	N_{PTF}
Partial asteroid models															
2778	Tangshan	−65	18			3.460693	19	4	0	169	0	130	263	0	0
11975	1995 FA1	65	9			6.21338	0	0	0	119	0	0	235	0	0
13066	1991 PM13	−57	19			3.93765	0	0	0	160	0	90	259	33	0
70184	1999 RU3	−59	14			5.27716	0	0	0	150	0	46	320	0	0

Notes. First, we list the new determinations, then the cases where we estimated only the ecliptic latitude of the spin axis (i.e., partial models). The table contains (i) physical properties – ecliptic longitudes and latitudes of the spin axis directions λ and β for one or two possible solutions, and sidereal rotation period P. For partial models, we show the mean value of the ecliptic latitude β_P and the 1/2 of the range in latitude within the multiple pole solutions $\delta\beta$. The uncertainty of the pole direction is usually about 10°and of the period of the order of the last decimal digit, and (ii) information about the lightcurve dataset – number of dense lightcurves N_{LC} with the number of covered apparitions N_{app}, and the number of measurements in each sparse dataset (N_{689}: UNSO-Flagstaff; N_{703}: CSS; N_{GAI}: Gaia DR2; N_{ASA}: ASAS-SN; N_{ATL}: ATLAS; N_{I41}: ZTF; N_{PTF}: PTF).

Table B.4. Updated shape models.

Number	Asteroid Name/Designation	λ_1 (deg)	β_1 (deg)	λ_2 (deg)	β_2 (deg)	P (h)	N_{LC}	N_{app}	N_{689}	N_{703}	N_{GAI}	N_{ASA}	N_{ATL}	N_{I41}	N_{PTF}
220	Stephania	36	−51			18.2087	9	2	137	242	12	376	599	30	0
249	Ilse	85	79	266	69	84.996	29	3	135	254	9	499	529	0	0
282	Clorinde	189	−36	346	−59	49.3597	29	2	175	197	13	659	548	0	0
370	Modestia	268	−92			22.5403	21	3	176	202	11	564	472	0	0
428	Monachia	98	90	283	53	3.633613	28	16	137	260	25	519	396	0	0
933	Susi	300	−9			4.62241	18	3	114	149	0	385	439	33	0
1216	Askania	62	55	260	66	6.53708	0	0	55	138	0	191	370	0	0
2012	Guo Shou-Jing	46	−79	230	−76	228.29	15	1	0	200	12	83	422	0	0
2536	Kozyrev	80	22	256	21	7.18887	3	1	27	138	14	348	494	0	0
2705	Wu	86	−70	265	−82	150.78	0	0	0	174	0	191	429	55	0
2772	Dugan	157	−71			235.76	1	1	0	174	0	120	360	0	0
2839	Annette	338	−47			10.46100	13	17	0	242	13	319	557	0	0
4231	Fireman	250	−83			339.57	16	1	26	228	13	248	511	88	0
4524	Barklajdetolli	76	70	257	93	966.5	19	2	0	175	0	188	391	0	0
5081	Sanguin	242	−39			10.26457	11	20	41	250	0	248	627	0	0
5524	Lecacheux	254	−86			8.41707	5	1	0	196	9	89	468	31	0
5924	Teruo	184	−60	359	−71	9.99174	6	1	20	153	13	217	447	0	0
9723	Binyang	36	45	215	38	12.38806	2	1	0	127	0	0	357	0	26
20771	2000 QY150	159	−63			8.30140	0	0	0	197	14	26	386	0	0
28736	2000 GE133	241	−65			4.65441	3	1	0	237	0	53	493	0	0

Notes. Same as in Table B.3.

Table B.5. Disk-integrated optical dense lightcurves utilized for the physical characterization of ancient family asteroids.

Epoch	N_p	Δ (AU)	r (AU)	φ (°)	Filter	Reference
				(220) Stephania		
1993-08-18.0	56	0.76	1.75	9.4	V	Mohamed et al. (1994)
1993-08-19.0	15	0.76	1.75	9.4	V	Mohamed et al. (1994)
1993-08-27.9	38	0.76	1.75	11.1	V	Mohamed et al. (1994)
1993-09-10.9	11	0.80	1.75	16.8	V	Mohamed et al. (1994)
1993-09-14.9	52	0.82	1.75	18.5	V	Mohamed et al. (1994)
1993-09-15.9	52	0.82	1.75	18.9	V	Mohamed et al. (1994)
2004-10-15.3	131	0.90	1.88	8.3	R	Robert A. Koff
2004-10-19.3	254	0.90	1.89	6.9	R	Robert A. Koff
2004-10-20.3	182	0.90	1.89	6.6	R	Robert A. Koff
				(249) Ilse		
1981-12-31.4	23	1.37	2.30	9.5	B	Binzel & Mulholland (1983)
1981-12-31.6	13	1.37	2.30	9.4	B	Binzel & Mulholland (1983)
1981-12-31.8	5	1.36	2.30	9.3	B	Binzel & Mulholland (1983)
1982-01-01.0	16	1.36	2.31	9.2	B	Binzel & Mulholland (1983)
1982-01-01.5	13	1.36	2.31	9.0	B	Binzel & Mulholland (1983)
1982-01-01.6	9	1.36	2.31	9.0	B	Binzel & Mulholland (1983)
1984-09-24.2	6	1.04	1.92	19.2	V	Binzel & Mulholland (1983)
2014-11-18.4	269	1.62	2.19	24.7	R	Pilcher (2015)
2014-11-19.4	274	1.61	2.20	24.5	R	Pilcher (2015)
2014-11-23.4	218	1.58	2.21	23.6	R	Pilcher (2015)
2014-11-24.4	193	1.57	2.21	23.4	R	Pilcher (2015)
2014-11-26.4	317	1.56	2.21	22.9	R	Pilcher (2015)
2014-11-28.4	306	1.54	2.22	22.4	R	Pilcher (2015)
2014-11-29.3	139	1.53	2.22	22.1	R	Pilcher (2015)
2014-11-29.5	168	1.53	2.22	22.0	R	Pilcher (2015)
2014-12-04.3	68	1.49	2.23	20.6	R	Pilcher (2015)
2014-12-13.4	266	1.44	2.25	17.5	R	Pilcher (2015)
2014-12-15.4	320	1.42	2.26	16.7	R	Pilcher (2015)
2014-12-17.3	174	1.41	2.26	15.9	R	Pilcher (2015)
2014-12-21.4	193	1.40	2.27	14.2	R	Pilcher (2015)
2014-12-31.3	343	1.36	2.30	9.8	R	Pilcher (2015)
2015-01-04.4	495	1.36	2.31	8.0	R	Pilcher (2015)
2015-01-12.2	221	1.36	2.33	5.0	R	Pilcher (2015)
2015-01-13.3	236	1.36	2.33	4.8	R	Pilcher (2015)
2015-01-17.3	518	1.37	2.34	4.4	R	Pilcher (2015)
2015-01-20.3	471	1.38	2.35	4.8	R	Pilcher (2015)
2015-01-26.2	325	1.40	2.36	6.6	R	Pilcher (2015)
2015-02-10.3	433	1.50	2.40	12.6	R	Pilcher (2015)
2015-02-13.2	438	1.53	2.41	13.7	R	Pilcher (2015)
(282) Clorinde						
1982-01-28.3	16	1.24	2.22	4.9	V	Binzel & Mulholland (1983)
1982-01-28.3	6	1.24	2.22	4.9	V	Binzel & Mulholland (1983)
2020-11-19.2	50	1.23	2.15	12.3	C	Roberto Bonamico
2020-11-26.2	105	1.20	2.15	9.6	C	Roberto Bonamico
2020-12-13.1	175	1.19	2.15	7.5	C	Roberto Bonamico
2020-12-16.2	16	1.19	2.15	8.4	C	Roberto Bonamico
2020-12-17.5	24	1.20	2.15	8.7	C	Roberto Bonamico
2020-12-19.5	19	1.20	2.15	9.3	C	Roberto Bonamico
2020-12-20.5	45	1.20	2.15	9.7	C	Roberto Bonamico
2020-12-21.5	30	1.21	2.15	10.1	C	Roberto Bonamico
2020-12-27.1	192	1.23	2.15	12.3	C	Roberto Bonamico
2020-12-05.5	20	1.19	2.15	7.2	C	Roberto Bonamico
2020-12-06.5	12	1.19	2.15	7.1	C	Roberto Bonamico
2020-12-07.5	11	1.19	2.15	7.0	C	Roberto Bonamico
2020-12-08.5	30	1.19	2.15	7.0	C	Roberto Bonamico
2021-01-10.4	32	1.32	2.15	17.9	C	Roberto Bonamico
2021-01-13.0	155	1.34	2.15	18.8	C	Roberto Bonamico
2021-01-15.2	8	1.36	2.15	19.7	C	Roberto Bonamico

Table B.5. continued.

Epoch	N_p	Δ (AU)	r (AU)	φ (°)	Filter	Reference
2021-01-16.4	44	1.37	2.15	19.9	C	Roberto Bonamico
2021-01-17.4	48	1.37	2.15	20.2	C	Roberto Bonamico
2021-01-18.2	10	1.38	2.15	20.6	C	Roberto Bonamico
2021-01-19.0	160	1.39	2.15	20.7	C	Roberto Bonamico
2021-01-03.4	27	1.27	2.15	15.3	C	Roberto Bonamico
2021-01-04.4	37	1.28	2.15	15.7	C	Roberto Bonamico
2021-02-10.9	85	1.62	2.16	25.7	C	Roberto Bonamico
2021-02-11.9	47	1.63	2.16	25.8	C	Roberto Bonamico
2021-02-07.3	12	1.58	2.15	25.2	C	Roberto Bonamico
2021-02-08.3	36	1.59	2.15	25.3	C	Roberto Bonamico
2021-03-06.3	17	1.90	2.16	27.3	C	Roberto Bonamico
(370) Modestia						
2003-08-30.1	45	1.13	2.13	5.9	R	Laurent Bernasconi
2003-09-21.1	47	1.22	2.12	15.8	R	Laurent Brunetto, Gilles Kober
2003-09-24.0	22	1.24	2.12	17.0	R	Laurent Brunetto, Gilles Kober
2010-07-21.4	190	1.20	2.18	9.1	R	Stephens (2011)
2010-07-22.4	178	1.19	2.18	8.6	R	Stephens (2011)
2010-07-23.4	187	1.19	2.18	8.1	R	Stephens (2011)
2010-07-24.4	199	1.18	2.18	7.6	R	Stephens (2011)
2010-07-25.4	174	1.18	2.18	7.2	R	Stephens (2011)
2010-07-28.3	133	1.17	2.17	5.7	R	Stephens (2011)
2010-07-29.4	186	1.17	2.17	5.2	R	Stephens (2011)
2010-07-30.3	187	1.16	2.17	4.8	R	Stephens (2011)
2010-07-31.4	303	1.16	2.17	4.3	R	Stephens (2011)
2010-08-02.4	156	1.16	2.17	3.5	R	Stephens (2011)
2010-08-04.3	199	1.16	2.17	2.9	R	Stephens (2011)
2021-08-17.1	153	1.46	2.11	25.5	C	NOAK
2021-08-28.2	75	1.36	2.11	22.9	r'	Stéphane Fauvaud, Marcel Fauvaud
2021-08-29.2	108	1.35	2.11	22.7	r'	Stéphane Fauvaud, Marcel Fauvaud
2021-08-31.2	133	1.34	2.11	22.1	r'	Stéphane Fauvaud, Marcel Fauvaud
2021-09-02.2	121	1.32	2.11	21.5	r'	Stéphane Fauvaud, Marcel Fauvaud
2021-09-07.2	146	1.28	2.12	19.9	r'	Stéphane Fauvaud, Marcel Fauvaud
2021-10-10.2	136	1.15	2.12	7.5	r'	Stéphane Fauvaud, Marcel Fauvaud
(428) Monachia						
1988-09-14.4	11	1.03	1.91	19.9	vV	Wisniewski et al. (1997)
1988-09-15.4	40	1.03	1.91	19.5	vV	Wisniewski et al. (1997)
1988-11-14.2	72	0.98	1.90	15.4	vV	Wisniewski et al. (1997)
1988-12-03.2	47	1.11	1.90	23.4	vV	Wisniewski et al. (1997)
1988-12-06.2	52	1.14	1.90	24.4	vV	Wisniewski et al. (1997)
1988-12-11.2	47	1.18	1.91	25.8	vV	Wisniewski et al. (1997)
1988-12-11.3	11	1.19	1.91	25.8	vV	Wisniewski et al. (1997)
2007-01-13.0	122	1.26	2.22	8.2	C	Pierre Antonini
2007-01-26.2	24	1.27	2.24	4.6	C	Agnieszka Kryszczyńska
2007-01-27.0	169	1.27	2.24	4.7	C	Pierre Antonini
2007-01-30.0	203	1.28	2.25	5.3	C	Pierre Antonini
2009-10-08.9	39	0.91	1.91	1.0	C	Kryszczyńska et al. (2012)
2009-11-21.7	18	1.09	1.90	22.7	C	Kryszczyńska et al. (2012)
2011-03-02.1	12	1.69	2.62	9.9	C	Anna Marciniak
2011-03-29.0	30	1.65	2.65	2.6	C	Kryszczyńska et al. (2012)
2014-03-17.2	50	1.68	2.34	21.8	V	Warner (2014)
2014-03-19.2	69	1.71	2.34	22.2	V	Warner (2014)
2016-10-01.9	142	0.92	1.91	3.3	C	Maurice Audejean
2016-10-05.9	125	0.91	1.91	0.9	C	Maurice Audejean
2016-10-18.2	50	0.92	1.90	7.1	R	Klinglesmith (2017)
2016-10-19.2	71	0.92	1.90	7.7	R	Klinglesmith (2017)
2016-10-19.3	61	0.92	1.90	7.8	R	Klinglesmith (2017)
2016-10-20.2	73	0.93	1.90	8.3	R	Klinglesmith (2017)
2016-10-20.3	68	0.93	1.90	8.4	R	Klinglesmith (2017)
2016-10-21.2	76	0.93	1.90	8.9	R	Klinglesmith (2017)
2016-10-21.3	42	0.93	1.90	9.0	R	Klinglesmith (2017)

Table B.5. continued.

Epoch	N_p	Δ (AU)	r (AU)	φ (°)	Filter	Reference
2016-10-22.2	74	0.93	1.90	9.5	R	Klinglesmith (2017)
2018-03-22.0	86	1.64	2.63	1.1	R	BE600
2019.7-2019.7	605	-	-	-	V	TESS
				(917) Lyka		
2018-10-03.9	90	0.95	1.95	3.8	V	Carreño et al. (2019)
2018-10-04.1	83	0.95	1.95	3.7	V	Carreño et al. (2019)
2018-10-04.9	98	0.95	1.95	3.4	V	Carreño et al. (2019)
2018-10-05.1	56	0.95	1.95	3.3	V	Carreño et al. (2019)
2018-10-05.2	24	0.95	1.95	3.3	V	Carreño et al. (2019)
2018-10-01.1	62	0.95	1.94	5.2	V	Matthieu Conjat
2018-10-19.0	78	0.98	1.97	7.2	V	Matthieu Conjat
2018-10-20.1	55	0.99	1.97	7.8	V	Matthieu Conjat
2018-10-25.0	73	1.01	1.97	10.4	V	Matthieu Conjat
2018-10-03.0	80	0.95	1.95	4.2	V	Matthieu Conjat
2018-10-04.1	100	0.95	1.95	3.7	V	Matthieu Conjat
2018-10-09.0	44	0.96	1.95	2.8	V	Matthieu Conjat
2018-11-13.9	7	1.16	2.00	19.4	V	Matthieu Conjat
				(933) Susi		
2011-01-08.7	12	1.48	1.98	28.7	R	David J. Higgins
2011-01-27.7	11	1.29	1.98	25.4	R	David J. Higgins
2011-01-29.7	24	1.27	1.98	24.9	R	David J. Higgins
2011-01-30.7	19	1.26	1.98	24.6	R	David J. Higgins
2011-01-31.7	26	1.25	1.98	24.4	R	David J. Higgins
2011-03-22.9	44	1.01	2.01	3.5	V	Strabla et al. (2011)
2011-03-23.9	53	1.02	2.01	3.6	V	Strabla et al. (2011)
2011-03-25.0	57	1.02	2.01	3.8	V	Strabla et al. (2011)
2011-04-09.1	103	1.06	2.02	10.7	R	Fauvaud & Fauvaud (2013)
2018-02-23.9	95	1.16	2.00	19.7	R	BE600
2020-11-10.0	37	1.64	2.55	11.4	C	Roberto Bonamico
2020-11-07.0	41	1.63	2.55	10.2	C	Roberto Bonamico
2020-11-08.9	26	1.64	2.55	11.0	C	Roberto Bonamico
2020-12-05.2	13	1.84	2.51	19.4	C	Roberto Bonamico
2020-12-06.3	46	1.85	2.51	19.6	C	Roberto Bonamico
2020-12-07.3	50	1.86	2.50	19.9	C	Roberto Bonamico
2021-01-10.2	21	2.23	2.45	23.7	C	Roberto Bonamico
2021-01-15.2	13	2.29	2.44	23.8	C	Roberto Bonamico
				(1159) Granada		
2021-10-20.7	319	1.39	2.36	6.0	C	UOAO
1984-09-23.3	6	1.31	2.29	7.7	V	Binzel (1987)
1984-09-24.3	5	1.31	2.29	8.2	V	Binzel (1987)
2021-10-22.0	102	1.39	2.37	6.0	C	UOAO
2021-10-27.1	371	1.40	2.37	6.9	C	C2PU
				(1244) Deira		
2007-02-03.6	7	1.45	2.12	23.9	R	Hanuš et al. (2016)
2007-02-05.6	26	1.43	2.12	23.4	R	Hanuš et al. (2016)
2007-02-09.6	35	1.39	2.11	22.5	R	Hanuš et al. (2016)
2007-02-14.6	51	1.34	2.11	21.2	R	Hanuš et al. (2016)
2007-02-15.5	24	1.34	2.11	20.9	R	Hanuš et al. (2016)
2007-02-17.6	49	1.32	2.11	20.3	R	Hanuš et al. (2016)
2007-02-23.6	54	1.27	2.11	18.3	R	Hanuš et al. (2016)
2007-03-03.6	46	1.22	2.11	15.3	R	Hanuš et al. (2016)
2007-03-09.6	31	1.19	2.11	13.0	R	Hanuš et al. (2016)
2007-03-11.0	124	1.18	2.11	12.6	R	Hanuš et al. (2016)
2007-03-11.5	46	1.18	2.11	12.2	R	Hanuš et al. (2016)
2007-03-15.5	49	1.16	2.11	10.7	R	Hanuš et al. (2016)
2007-03-23.1	21	1.15	2.11	8.5	R	Hanuš et al. (2016)
2007-03-23.6	65	1.14	2.11	8.3	R	Hanuš et al. (2016)
2007-03-27.6	10	1.14	2.12	7.7	R	Hanuš et al. (2016)
2007-03-28.6	30	1.14	2.12	7.6	R	Hanuš et al. (2016)
2007-03-30.6	44	1.14	2.12	7.6	R	Hanuš et al. (2016)

Table B.5. continued.

Epoch	N_p	Δ (AU)	r (AU)	φ (°)	Filter	Reference
2007-03-31.4	12	1.14	2.12	7.7	R	Hanuš et al. (2016)
2007-04-01.6	57	1.14	2.12	7.8	R	Hanuš et al. (2016)
(1700) Zvezdara						
2009-08-20.7	37	0.95	1.87	18.6	R	Baker et al. (2010)
2009-08-27.7	55	0.91	1.86	15.3	R	Baker et al. (2010)
2009-09-12.6	43	0.85	1.84	6.1	R	Baker et al. (2010)
2009-09-15.6	55	0.84	1.84	4.2	R	Baker et al. (2010)
2009-09-18.2	130	0.84	1.84	2.4	R	Baker et al. (2010)
2009-09-24.9	75	0.83	1.84	2.0	R	Baker et al. (2010)
2009-09-26.9	76	0.84	1.84	3.2	R	Baker et al. (2010)
2009-09-28.9	60	0.84	1.83	4.5	R	Baker et al. (2010)
2009-09-30.3	210	0.84	1.83	5.4	R	Baker et al. (2010)
2009-09-30.9	72	0.84	1.83	5.8	R	Baker et al. (2010)
2009-10-04.9	68	0.85	1.83	8.3	R	Baker et al. (2010)
2009-10-05.9	68	0.85	1.83	9.0	R	Baker et al. (2010)
2009-10-06.9	70	0.85	1.83	9.6	R	Baker et al. (2010)
2009-10-07.9	62	0.86	1.83	10.2	R	Baker et al. (2010)
2009-10-08.9	78	0.86	1.83	10.8	R	Baker et al. (2010)
2009-10-11.1	19	0.87	1.83	12.1	R	Baker et al. (2010)
2009-10-19.1	72	0.90	1.83	16.5	R	Baker et al. (2010)
2020-11-19.0	75	0.95	1.88	15.1	C	Roberto Bonamico
2020-11-23.0	61	0.98	1.88	17.0	C	Roberto Bonamico
2020-12-16.2	33	1.19	1.92	25.2	C	Roberto Bonamico
2020-12-19.3	34	1.22	1.92	25.9	C	Roberto Bonamico
2020-12-06.4	56	1.09	1.90	22.3	C	Roberto Bonamico
2020-12-07.4	59	1.10	1.90	22.6	C	Roberto Bonamico
2020-12-08.4	35	1.11	1.91	23.0	C	Roberto Bonamico
2021-01-15.2	13	1.53	1.98	29.2	C	Roberto Bonamico
2021-01-16.3	28	1.55	1.98	29.3	C	Roberto Bonamico
2021-01-16.8	15	1.56	1.98	29.3	C	Roberto Bonamico
2021-01-17.9	26	1.57	1.98	29.3	C	Roberto Bonamico
2021-01-03.3	44	1.39	1.95	28.3	C	Roberto Bonamico
2021-01-04.3	42	1.40	1.95	28.4	C	Roberto Bonamico
(1806) Derice						
2020-02-05.2	30	1.79	2.03	29.1	SR	Stephens & Warner (2020)
2020-02-06.2	26	1.80	2.02	29.1	SR	Stephens & Warner (2020)
2020-02-07.2	9	1.81	2.02	29.1	SR	Stephens & Warner (2020)
2020-02-08.2	23	1.82	2.02	29.1	SR	Stephens & Warner (2020)
2020-02-12.2	32	1.86	2.02	29.1	SR	Stephens & Warner (2020)
2020-02-13.2	44	1.87	2.02	29.1	SR	Stephens & Warner (2020)
2020-02-14.2	43	1.88	2.02	29.0	SR	Stephens & Warner (2020)
2020-02-15.2	41	1.90	2.02	29.0	SR	Stephens & Warner (2020)
2020-02-16.2	26	1.91	2.02	29.0	SR	Stephens & Warner (2020)
2020-02-17.2	17	1.92	2.02	28.9	SR	Stephens & Warner (2020)
2020-02-18.2	6	1.93	2.02	28.9	SR	Stephens & Warner (2020)
2020-02-19.2	39	1.94	2.02	28.9	SR	Stephens & Warner (2020)
2020-02-20.2	33	1.95	2.02	28.8	SR	Stephens & Warner (2020)
2020-02-21.2	37	1.96	2.02	28.8	SR	Stephens & Warner (2020)
2021-05-19.0	53	1.36	2.35	7.3	C	Roberto Bonamico
2021-05-04.1	40	1.33	2.33	2.2	C	Roberto Bonamico
2021-05-06.1	56	1.33	2.34	2.1	C	Roberto Bonamico
(1924) Horus						
2021-10-12.1	35	1.47	2.45	4.5	C	Andrea Ferrero
2021-10-15.1	44	1.46	2.45	3.1	C	Andrea Ferrero
2021-10-07.2	31	1.49	2.46	6.8	C	Andrea Ferrero
2021-11-02.0	46	1.45	2.42	6.3	C	Andrea Ferrero
2021-11-05.1	47	1.46	2.42	7.8	C	Andrea Ferrero
2021-09-30.2	17	1.52	2.47	9.9	C	Andrea Ferrero
(2012) Guo Shou-Jing						
2021-10-17.2	80	1.27	2.21	11.2	C	Andrea Ferrero

Table B.5. continued.

Epoch	N_p	Δ (AU)	r (AU)	φ (°)	Filter	Reference
2021-10-26.1	9	1.26	2.23	6.5	C	Andrea Ferrero
2021-10-27.2	42	1.25	2.23	6.0	C	Andrea Ferrero
2021-10-28.1	18	1.25	2.23	5.5	C	Andrea Ferrero
2021-11-23.9	23	1.35	2.29	9.4	C	Andrea Ferrero
2021-11-29.0	56	1.38	2.30	11.7	C	Andrea Ferrero
2021-11-30.0	58	1.39	2.30	12.1	C	Andrea Ferrero
2021-12-10.0	63	1.48	2.32	16.0	C	Andrea Ferrero
2021-12-01.0	54	1.40	2.30	12.5	C	Andrea Ferrero
2021-12-29.9	29	1.72	2.36	21.3	C	Andrea Ferrero
2021-12-03.0	57	1.42	2.31	13.4	C	Andrea Ferrero
2021-12-04.0	53	1.43	2.31	13.8	C	Andrea Ferrero
2021-12-05.0	46	1.43	2.31	14.2	C	Andrea Ferrero
2021-12-06.0	65	1.44	2.31	14.5	C	Andrea Ferrero
2021-12-07.0	61	1.45	2.32	14.9	C	Andrea Ferrero
(2171) Kiev						
2020-05-23.9	226	0.96	1.96	7.6	V	Rafael González
2020-05-26.9	88	0.97	1.96	8.9	GG	Rafael González
2020-05-29.9	134	0.97	1.95	10.3	GG	Rafael González
2020-06-01.9	90	0.97	1.95	11.7	GG	Rafael González
2022-01-20.9	45	1.99	2.58	20.1	C	Andrea Ferrero
2022-01-07.0	58	1.82	2.57	17.1	C	Andrea Ferrero
2022-01-08.0	58	1.83	2.57	17.4	C	Andrea Ferrero
(2322) Kitt Peak						
2020-11-10.2	24	1.21	2.20	1.2	C	Roberto Bonamico
2020-11-11.2	23	1.21	2.20	1.1	C	Roberto Bonamico
2020-11-18.0	49	1.22	2.21	4.1	C	Roberto Bonamico
2020-11-07.2	18	1.22	2.20	2.4	C	Roberto Bonamico
2020-12-16.3	34	1.38	2.21	17.4	C	Roberto Bonamico
2020-12-17.4	57	1.39	2.21	17.8	C	Roberto Bonamico
2020-12-19.2	27	1.41	2.21	18.5	C	Roberto Bonamico
2020-12-20.4	54	1.42	2.21	18.8	C	Roberto Bonamico
2020-12-05.4	37	1.30	2.21	12.9	C	Roberto Bonamico
2020-12-06.4	62	1.31	2.21	13.3	C	Roberto Bonamico
2020-12-07.4	67	1.31	2.21	13.8	C	Roberto Bonamico
2020-12-08.4	43	1.32	2.21	14.2	C	Roberto Bonamico
2021-01-04.3	43	1.57	2.22	22.9	C	Roberto Bonamico
(2536) Kozyrev						
2011-03-13.3	37	1.80	2.71	10.5	SR	Skiff et al. (2019)
2011-03-14.2	59	1.81	2.71	10.8	SR	Skiff et al. (2019)
2011-03-24.2	37	1.90	2.72	14.2	SR	Skiff et al. (2019)
(2575) Bulgaria						
2021-11-05.2	29	1.59	2.51	10.7	C	Andrea Ferrero
2021-11-06.2	53	1.59	2.51	10.4	C	Andrea Ferrero
2021-11-07.1	42	1.58	2.51	10.0	C	Andrea Ferrero
2021-12-12.1	40	1.57	2.52	7.9	C	Andrea Ferrero
2021-12-13.1	73	1.57	2.52	8.3	C	Andrea Ferrero
(2768) Gorky						
2019-09-15.0	59	1.32	1.85	31.6	R	Benishek (2020)
2019-09-16.1	63	1.31	1.85	31.5	R	Benishek (2020)
2019-12-13.9	128	0.97	1.93	9.7	C	UOAO
2019-12-16.1	299	0.98	1.93	10.8	C	UOAO
2019-12-17.0	476	0.99	1.93	11.4	C	UOAO
2019-12-18.1	233	0.99	1.94	12.0	C	UOAO
2019-12-20.9	122	1.01	1.94	13.6	C	UOAO
2021-03-23.2	45	1.69	2.61	10.7	C	Roberto Bonamico
2021-04-14.0	35	1.61	2.62	2.0	C	UOAO
2021-04-15.0	14	1.61	2.62	1.8	C	UOAO
2021-04-20.0	74	1.62	2.62	2.8	C	UOAO
2021-04-21.0	93	1.62	2.62	3.2	C	UOAO
2021-04-06.1	69	1.63	2.61	4.8	C	Roberto Bonamico

Table B.5. continued.

Epoch	N_p	Δ (AU)	r (AU)	φ (°)	Filter	Reference
2021-04-08.1	74	1.62	2.61	4.0	C	Roberto Bonamico
2021-04-09.1	65	1.62	2.61	3.6	C	Roberto Bonamico
2021-05-06.1	82	1.67	2.62	9.5	C	Andrea Ferrero
2021-05-07.1	79	1.67	2.62	9.9	C	Andrea Ferrero
2021-05-08.0	48	1.68	2.62	10.4	C	Andrea Ferrero
(2772) Dugan						
2007-12-07.6	13	0.88	1.84	9.8	R	Julian Oey
(2773) Brooks						
2018-12-10.0	90	1.14	2.09	9.7	L	Matthieu Conjat
2018-12-08.1	109	1.15	2.09	10.8	L	Matthieu Conjat
2018-12-09.1	89	1.14	2.09	10.2	L	Matthieu Conjat
2021-10-11.0	21	1.22	2.07	19.3	C	Roberto Bonamico
2021-10-06.9	24	1.20	2.07	17.7	C	Roberto Bonamico
2021-09-24.9	20	1.14	2.09	12.2	C	Roberto Bonamico
2021-09-30.0	34	1.16	2.08	14.6	C	Roberto Bonamico
(2776) Baikal						
2007-01-16.5	25	1.02	1.99	7.4	R	Julian Oey
(2778) Tangshan						
2003-11-26.3	131	1.08	2.07	2.6	R	Warner (2004)
2003-11-28.3	115	1.09	2.07	3.4	R	Warner (2004)
2018-01-20.1	24	1.30	2.23	11.1	C	Matthieu Conjat
2018-01-20.9	35	1.31	2.23	11.5	C	Matthieu Conjat
2018-01-21.9	36	1.32	2.23	11.9	C	Matthieu Conjat
2018-01-22.9	19	1.32	2.24	12.4	C	Matthieu Conjat
2018-01-23.8	17	1.33	2.24	12.8	C	Matthieu Conjat
2019-06-09.3	21	1.71	2.51	17.2	V	Stephens & Warner (2019a)
2019-06-10.3	52	1.72	2.51	17.5	V	Stephens & Warner (2019a)
2019-06-11.2	31	1.72	2.51	17.8	V	Stephens & Warner (2019a)
2020-11-11.0	64	1.16	2.01	19.2	C	Roberto Bonamico
2020-11-15.0	36	1.19	2.01	20.7	C	Roberto Bonamico
2020-11-16.9	17	1.21	2.01	21.4	C	Roberto Bonamico
2020-12-19.3	7	1.53	2.02	28.1	C	Roberto Bonamico
2020-12-31.1	6	1.67	2.03	28.8	C	Roberto Bonamico
2020-12-08.3	33	1.41	2.02	26.7	C	Roberto Bonamico
2021-01-10.1	7	1.79	2.03	28.9	C	Roberto Bonamico
2021-01-15.2	8	1.85	2.04	28.8	C	Roberto Bonamico
2021-02-08.2	17	2.14	2.06	27.1	C	Roberto Bonamico
(2792) Ponomarev						
2019.6-2019.7	228	-	-	-	V	TESS
(2839) Annette						
2005-10-30.4	23	0.90	1.89	1.3	V	Buchheim (2007)
2005-10-31.3	30	0.90	1.89	1.8	V	Buchheim (2007)
2005-11-01.3	27	0.90	1.89	2.4	V	Buchheim (2007)
2005-12-15.1	35	1.12	1.88	24.8	R	Warner (2006)
2005-12-16.1	41	1.13	1.88	25.1	R	Warner (2006)
2005-12-19.2	18	1.16	1.88	26.0	R	Warner (2006)
2005-12-21.1	12	1.18	1.88	26.5	R	Warner (2006)
2005-12-22.2	48	1.18	1.88	26.7	R	Warner (2006)
2018.8-2018.9	1204	-	-	-	V	TESS
2020-04-17.0	68	1.51	2.44	11.3	C	UOAO
2020-04-19.0	82	1.53	2.44	12.1	C	UOAO
2020-04-23.9	54	1.57	2.45	14.1	C	UOAO
2020-04-24.9	22	1.57	2.45	14.5	C	UOAO
2020-04-26.0	63	1.58	2.45	14.8	C	UOAO
(3633) Mira						
2021-11-30.1	16	1.48	2.18	22.2	C	Andrea Ferrero
2021-12-01.2	39	1.47	2.18	22.0	C	Andrea Ferrero
2021-12-13.2	27	1.35	2.17	18.3	C	Andrea Ferrero
2021-12-14.2	37	1.34	2.17	18.0	C	Andrea Ferrero
2021-12-15.2	53	1.33	2.17	17.6	C	Andrea Ferrero

Table B.5. continued.

Epoch	N_p	Δ (AU)	r (AU)	φ (°)	Filter	Reference
2021-12-16.2	28	1.32	2.16	17.2	C	Andrea Ferrero
2021-12-03.2	41	1.45	2.18	21.5	C	Andrea Ferrero
2021-12-06.2	42	1.42	2.18	20.6	C	Andrea Ferrero
2021-12-07.2	37	1.41	2.17	20.3	C	Andrea Ferrero
2022-01-10.2	60	1.17	2.14	5.6	C	Andrea Ferrero
2022-01-01.1	24	1.21	2.15	10.2	C	Andrea Ferrero
2022-01-11.2	55	1.17	2.14	5.1	C	Andrea Ferrero
(3723) Voznesenskij						
2021-10-24.0	112	1.38	2.35	6.4	C	C2PU
2021-10-25.0	55	1.38	2.35	6.9	C	C2PU
2021-10-27.7	57	1.40	2.36	8.3	C	Helmos
(4024) Ronan						
2010-01-09.5	109	1.00	1.93	12.5	R	Stephens & Warner (2010)
2010-01-24.4	97	0.96	1.93	7.6	R	Stephens & Warner (2010)
2010-01-28.4	129	0.96	1.93	7.7	R	Stephens & Warner (2010)
2010-01-31.4	67	0.96	1.93	8.3	R	Stephens & Warner (2010)
2010-02-04.3	187	0.97	1.93	9.4	R	Stephens & Warner (2010)
2010-02-09.2	143	0.98	1.93	11.4	R	Stephens & Warner (2010)
2010-02-11.3	189	0.99	1.93	12.3	R	Stephens & Warner (2010)
2010-02-13.3	221	0.99	1.93	13.2	R	Stephens & Warner (2010)
2010-02-14.3	216	1.00	1.93	13.6	R	Stephens & Warner (2010)
2010-02-15.3	184	1.00	1.93	14.1	R	Stephens & Warner (2010)
2010-02-15.3	89	1.00	1.93	14.1	R	Stephens & Warner (2010)
2010-02-16.3	160	1.01	1.93	14.6	R	Stephens & Warner (2010)
2010-02-17.3	169	1.01	1.93	15.0	R	Stephens & Warner (2010)
2010-02-18.2	166	1.01	1.93	15.5	R	Stephens & Warner (2010)
2010-02-21.3	210	1.03	1.93	16.8	R	Stephens & Warner (2010)
2010-02-23.3	102	1.04	1.93	17.7	R	Stephens & Warner (2010)
2010-02-24.3	111	1.05	1.93	18.1	R	Stephens & Warner (2010)
2010-03-04.2	40	1.10	1.93	21.3	R	Stephens & Warner (2010)
2010-03-13.2	56	1.17	1.94	24.3	R	Stephens & Warner (2010)
(4231) Fireman						
2020-12-16.2	33	1.31	2.26	8.0	C	Roberto Bonamico
2020-12-17.5	71	1.32	2.27	8.5	C	Roberto Bonamico
2020-12-19.5	44	1.33	2.27	9.5	C	Roberto Bonamico
2020-12-20.4	64	1.33	2.27	10.0	C	Roberto Bonamico
2020-12-21.4	63	1.34	2.27	10.5	C	Roberto Bonamico
2020-12-05.5	29	1.27	2.26	2.5	C	Roberto Bonamico
2020-12-06.5	73	1.28	2.26	2.8	C	Roberto Bonamico
2020-12-07.5	76	1.28	2.26	3.3	C	Roberto Bonamico
2020-12-08.5	58	1.28	2.26	3.9	C	Roberto Bonamico
2021-01-10.4	24	1.50	2.28	18.5	C	Roberto Bonamico
2021-01-16.4	42	1.56	2.29	20.3	C	Roberto Bonamico
2021-01-17.4	51	1.58	2.29	20.6	C	Roberto Bonamico
2021-01-18.2	20	1.59	2.29	20.8	C	Roberto Bonamico
2021-01-03.4	58	1.44	2.28	16.1	C	Roberto Bonamico
2021-01-04.4	60	1.44	2.28	16.5	C	Roberto Bonamico
2021-03-03.3	7	2.15	2.32	25.3	C	Roberto Bonamico
(4524) Barklajdetolli						
2009-06-17.3	21	1.21	2.06	20.3	V	Pray & Durkee (2010)
2009-07-13.3	60	1.05	2.04	9.8	V	Pray & Durkee (2010)
2009-07-15.2	33	1.05	2.04	9.0	V	Pray & Durkee (2010)
2009-07-19.2	16	1.04	2.03	7.4	V	Pray & Durkee (2010)
2009-07-26.2	225	1.03	2.03	5.8	V	Pray & Durkee (2010)
2009-07-26.3	37	1.03	2.03	5.8	V	Pray & Durkee (2010)
2009-07-26.3	43	1.03	2.03	5.8	V	Pray & Durkee (2010)
2009-07-26.3	48	1.03	2.03	5.8	V	Pray & Durkee (2010)
2009-07-26.3	50	1.03	2.03	5.8	V	Pray & Durkee (2010)
2009-07-31.2	17	1.02	2.03	6.2	V	Pray & Durkee (2010)
2009-08-02.2	10	1.03	2.03	6.7	V	Pray & Durkee (2010)

Table B.5. continued.

Epoch	N_p	Δ (AU)	r (AU)	φ (°)	Filter	Reference
2009-08-02.2	9	1.03	2.03	6.8	V	Pray & Durkee (2010)
2009-08-11.3	135	1.04	2.02	10.3	V	Pray & Durkee (2010)
2009-08-12.3	104	1.05	2.02	10.8	V	Pray & Durkee (2010)
2009-08-29.2	6	1.13	2.02	18.3	V	Pray & Durkee (2010)
2016-06-18.0	15	1.14	2.09	13.7	V	Benishek (2017)
2016-06-19.0	5	1.13	2.09	13.3	V	Benishek (2017)
2016-06-24.0	6	1.11	2.08	11.2	V	Benishek (2017)
2016-09-01.9	6	1.29	2.03	24.7	V	Benishek (2017)
(5081) Sanguin						
2010-03-25.3	87	1.28	2.21	12.6	R	Warner (2010)
2010-04-03.2	24	1.31	2.20	15.5	R	Warner (2010)
2010-04-05.2	12	1.32	2.20	16.1	R	Warner (2010)
2010-04-09.3	70	1.34	2.19	17.5	R	Warner (2010)
2010-04-10.3	58	1.34	2.19	17.8	R	Warner (2010)
2018.8-2018.9	1198	-	-	-	V	TESS
2021-05-15.1	45	1.07	2.06	8.3	C	Roberto Bonamico
2021-05-17.1	53	1.06	2.06	7.3	C	Roberto Bonamico
2021-05-18.1	78	1.06	2.06	6.8	C	Roberto Bonamico
2021-05-19.1	48	1.06	2.06	6.3	C	Roberto Bonamico
2021-06-14.0	33	1.08	2.06	10.8	C	Roberto Bonamico
2021-06-15.0	25	1.08	2.06	11.3	C	Roberto Bonamico
(5333) Kanaya						
2010-04-13.6	59	1.11	2.08	9.0	R	Higgins (2011)
2010-04-21.6	63	1.10	2.09	4.6	R	Higgins (2011)
2010-05-06.6	44	1.12	2.12	4.9	R	Higgins (2011)
2010-05-15.0	128	1.16	2.13	9.4	C	René Roy
2010-05-20.0	56	1.18	2.14	11.8	C	René Roy
2021-06-15.1	65	1.36	2.35	8.1	C	C2PU
2021-06-16.1	102	1.37	2.35	8.4	C	C2PU
2021-06-19.0	93	1.38	2.36	9.4	C	C2PU
2021-07-12.0	17	1.56	2.40	17.2	C	S. Fauvaud, J.-J. Rives, S. Brouillard, F. Livet
(5524) Lecacheux						
2012-04-29.3	62	1.31	2.30	6.6	R	J. W. Brinsfield
2012-05-10.3	14	1.34	2.30	10.6	R	J. W. Brinsfield
2012-05-15.3	10	1.37	2.30	12.6	R	J. W. Brinsfield
2012-05-16.3	12	1.37	2.30	13.0	R	J. W. Brinsfield
2012-05-24.3	10	1.42	2.30	16.0	R	J. W. Brinsfield
(5924) Teruo						
2012-03-10.3	114	1.11	2.10	4.4	R	J. W. Brinsfield
2012-03-13.3	54	1.11	2.09	5.8	R	J. W. Brinsfield
2012-03-20.2	29	1.13	2.09	9.3	R	J. W. Brinsfield
2012-03-21.2	22	1.13	2.09	9.9	R	J. W. Brinsfield
2012-03-22.2	35	1.14	2.09	10.3	R	J. W. Brinsfield
2012-04-09.2	42	1.23	2.09	18.6	R	J. W. Brinsfield
(6125) Singto						
2022-01-12.2	61	1.36	2.33	5.1	C	Andrea Ferrero
2022-01-07.2	48	1.37	2.32	7.7	C	Andrea Ferrero
2022-01-08.2	33	1.37	2.33	7.2	C	Andrea Ferrero
(6647) Josse						
2018-08-03.0	43	0.85	1.82	13.4	C	Matthieu Conjat
2018-08-04.0	45	0.85	1.82	12.8	C	Matthieu Conjat
2018-08-05.0	25	0.84	1.82	12.3	C	Matthieu Conjat
2018-08-09.0	40	0.83	1.82	9.9	C	Matthieu Conjat
2018-08-16.1	33	0.80	1.81	5.6	C	Matthieu Conjat
2018-08-30.0	29	0.79	1.80	4.0	C	Matthieu Conjat
(9723) Binyang						
1990-02-28.2	25	1.54	2.39	15.0	V-	Binzel et al. (1992)
1990-03-01.2	16	1.55	2.39	15.4	V-	Binzel et al. (1992)
(28736) 2000 GE133						
2007-05-12.6	12	1.25	2.23	8.1	R	Higgins (2008)

Table B.5. continued.

Epoch	N_p	Δ (AU)	r (AU)	φ (°)	Filter	Reference
2007-05-13.6	37	1.25	2.23	7.9	R	Higgins (2008)
2007-05-14.6	45	1.25	2.23	7.8	R	Higgins (2008)

Notes. For each lightcurve, the table gives the epoch, the number of individual measurements N_p, asteroid's distances to the Earth Δ and the Sun r, phase angle φ, photometric filter and the reference to the data.